2.03 Mineralogy of the Earth – Phase Transitions and Mineralogy of the Lower Mantle

T. Irifune and T. Tsuchiya, Ehime University, Matsuyama, Japan

2.03.1 Introduction

Until recently, experimental high-pressure mineral physics studies mainly focused on materials in the upper part of the mantle, because of technical restrictions in pressure and temperature generation and also in precise measurements of crystal structures and physical properties under the lower-mantle conditions. However, developments in technologies of both laser-heated diamond-anvil cell (LHDAC) and large-volume Kawai-type multianvil apparatus (KMA), combined with synchrotron radiation, have enabled us to quantitatively study phase transitions and some key physical properties of mantle minerals under the P,T conditions encompassing those of the whole mantle.

Progress in computational mineral physics based on *ab initio* calculations has also been dramatic in the last decade in conjunction with the rapid advancement of computer technologies. Classical molecular dynamics calculations required *a priori* assumptions on the

parameters for interatomic model potentials, which largely rely on available experimental data. Quantum mechanical Hamiltonians of many-body electron systems can be efficiently and quantitatively evaluated on the basis of the density functional theory (DFT) (Hohenberg and Kohn, 1964; Kohn and Sham, 1965). Practical calculations of minerals having complex crystal structures can be achieved using various methods and techniques developed following the DFT. As a result of such advancement in *ab initio* calculations, it is now possible to predict stability and some physical properties of high-pressure forms quantitatively with uncertainties that are even comparable to those attached in experimentally derived data, as was dramatically shown in a series of recent articles relevant to the postperovskite phase transition (Tsuchiya *et al.*, 2004a, 2004b; Oganov and Ono, 2004; Iitaka *et al.*, 2004).

Another reason for the relatively scarce mineral physics studies for the lower part of the mantle may originate from the fact that there has been no indication of the occurrence of major phase transitions under these conditions, except for those corresponding to uppermost (~660–800 km) and lowermost (~2700–2900 km; the D″ layer) parts of the lower mantle. This is in marked contrast to the nature of the mantle transition region, best described as "the key to a number of geophysical problems" by Birch (1952). Recent seismological studies, however, demonstrated that there are regions that significantly scatter seismic waves, which may be related to some unknown phase transitions and/or chemical boundaries at certain depths in the upper to middle regions of the lower mantle (e.g., Niu and Kawakatsu, 1996). In addition, both geochemical considerations and mantle dynamics simulations suggest that the mantle may be divided into chemically distinct regions by a boundary at 1500–2000 km depths in the lower mantle (e.g., Kellogg *et al.*, 1999; Tackley, 2000; Trampert *et al.*, 2004). Moreover, seismological studies with various methods of analysis have shown detailed structures in the D″ layer, demonstrating marked heterogeneity in both horizontal and vertical directions (Lay *et al.*, 2004). Thus, there is growing evidence that the lower mantle is not featureless any more, and many mineral physicists have started to develop experimental and computational techniques for higher pressure and temperature conditions (with improved accuracy) in order to elucidate the mineralogy of the lower mantle.

In spite of the great efforts in both experimental and theoretical studies (mostly conducted in the last decade), our knowledge on the stability and mineral physics properties of high-pressure phases relevant to the lower mantle is still very limited compared with that on the shallower parts of the mantle. Although LHDACs are now capable of generating pressures and temperatures corresponding to, or even beyond, the mantle–core boundary, there remain a number of disagreements in phase equilibrium studies using this method with various techniques in heating, temperature/pressure measurements, phase identification, etc. Mineral physics parameters that constrain densities of high-pressure phases in the lower mantle have been accumulated thanks to the intense synchrotron sources, particularly those available at third-generation synchrotron facilities, such as ESRF, APS, and SPring-8, combined with both LHDAC and KMA, but those related to elastic wave velocities are scarce to date.

In the present chapter, we briefly review recent progress and limitations in experimental and computational techniques in studying phase transitions and some key physical properties under the lower-mantle conditions. Then we summarize current knowledge on these properties obtained experimentally and/or theoretically using these techniques. We rather focus on the phase transitions and phase relations in simple silicates, oxides, carbonates, and hydrous systems closely related to the mantle and slab materials, because experimental measurements or theoretical predictions of other properties such as shear moduli and their pressure/temperature dependency are still limited for lower-mantle conditions. In contrast, equation of state (EoS) parameters, that is, zero-pressure densities, bulk moduli, and their pressure/temperature dependencies of some of the high-pressure phases are summarized, as far as reliable data are available. We also review the phase transitions and density changes in lithologies associated with the subduction of slabs and also those in the surrounding model mantle materials on the basis of experimental results on multicomponent systems. Some implications for the mineralogy of the lower mantle are discussed based on these data and those obtained for the simpler systems.

2.03.2 Experimental and Theoretical Backgrounds

2.03.2.1 High-Pressure Technology

Two kinds of high-pressure devices, LHDAC and KMA, have been used to realize static high-pressure and high-temperature conditions of the lower mantle in the laboratory. The upper limit of high-pressure generation in LHDAC has been dramatically

expanded using a smaller anvil top (culet) with various shapes for utilizing the potential hardness of single-crystal diamond. As a result, generation of pressures of multimegabars can now be comfortably produced in some laboratories. Moreover, quasihydrostatic pressures are also available by introducing gas pressure media, such as Ar or He, which also serve as thermal insulators in heating samples with laser beams.

The quality of heating of samples in LHDAC has also been substantially improved using various laser sources, such as YAG, CO_2, and YLF, with higher powers and more sophisticated computer-controlled feedback systems, as compared with the laser heating in early stages of its development in the 1970s and 1980s. These can now yield stable high temperature in a sample as small as ~100 to several tens of micrometers in diameter and even smaller thickness.

Pressures produced in KMA studies (Kawai and Endo, 1970) using conventional tungsten carbide anvils have long been limited to 25–30 GPa, although the relatively large sample volume in this apparatus made it possible to precisely determine the phase transitions, some physical properties, melting temperatures, element partitioning, etc., of high-pressure phases. Temperatures up to 3000 K are also produced stably for hours or even a few days using various forms of heaters, such as C, $LaCrO_3$, TiC, WC, and some refractory metals. In addition, both temperature and pressure gradients within the sample in KMA are believed to be far smaller than those in LHDAC.

Introduction of harder materials, that is, sintered bodies of polycrystalline diamonds (SD) with some binders, such as Co and Si, as the second-stage anvils of KMA has dramatically changed this situation. Using relatively large SD anvil cubes of over 10 mm in edge length, some laboratories are now able to produce pressures approaching 60 GPa at high temperatures using KMA (e.g., Ito *et al.*, 2005), without sacrificing the advantage of the relatively large sample volumes in this apparatus. It is expected that pressures as high as ~100 GPa may be produced in KMA, if SD anvils with larger dimensions are supplied on a commercial basis.

Applications of synchrotron radiation to both LHDAC and KMA started in the mid-1980s, when the second-generation synchrotron sources became available worldwide (e.g., Shimomura *et al.*, 1984). A combination of white X-ray and an energy-dispersive system has been used for KMA experiments at synchrotron facilities, because geometrical constraints imposed by the tungsten carbide anvils and surrounding guide-block systems make it difficult to conduct angle-dispersive diffraction measurements. Use of the energy-dispersive method combined with a multichannel analyzer has the merit of rapid acquisition and analysis of X-ray diffraction data, so that realtime observations of phase transitions are possible under high pressure and high temperature. Although this method is not very suitable for the precise determination of crystal structures (due to relatively low spatial resolutions in the diffraction peak position and also to significant variations in background X-ray with the energy range), some attempts have been successfully made to make crystal structure refinements using a combined step scanning and energy-dispersive measurements (Wang *et al.*, 2004).

Identification of the phases present and precise determinations of the lattice parameters, and hence unit-cell volumes, of the high-pressure phases can be made by *in situ* X-ray diffraction measurements. The *in situ* pressure can also be monitored by the unit-cell volume changes in some reference materials, such as NaCl, Au, Pt, and MgO, using an appropriate EoS. Thus the phase boundaries and the P,V,T relations of a number of high-pressure phases relevant to lower-mantle mineralogy have been determined by *in situ* X-ray measurements using KMA, although there remain some uncertainties in the estimated pressures due to the lack of reliable pressure scales, as reviewed later, particularly at pressures of the deeper parts of the lower mantle. The effect of pressure on the electromotive force of a thermocouple is another unresolved issue, which may yield an additional uncertainty in the pressure estimation based on these EoS's.

Corresponding *in situ* X-ray observations have also been made using LHDAC. As the geometrical restrictions on the X-ray paths are not so severe in this device, X-ray diffraction is measured with an angle-dispersion method using monochromatized X-ray. The X-ray beam is focused to generally ~10–20 μm with collimating mirrors, and directed to the disk-shape sample with diameters of ~20–200 μm, depending on pressure ranges. YAG or ILF lasers with beam sizes of ~10 to several tens of micrometers are used in most of the synchrotron facilities. By adopting imaging plates (IPs) for X-ray exposure combined with data processing systems, rapid data acquisition and reductions are also possible. Thus, the phase identification and measurements of unit-cell parameters of high-pressure phases can be made by the combination of LHDAC and

synchrotron radiation at pressure and temperature conditions corresponding to the entire mantle (e.g., Murakami *et al.*, 2004a).

The major uncertainty in the *in situ* X-ray observations with LHDAC arises from the possible large temperature gradients in the small thin sample. Some studies demonstrated that variations of temperature are not very large in the radial direction of the disk-shape sample, suggesting that the temperature uncertainty may be of the order of ~10% or less of the nominal values, if the diameter of the laser beam is significantly larger than that of the X-ray beam (Shen *et al.*, 2001). However, the temperature gradient in the axial direction of the sample can be substantially larger than this estimation (Irifune *et al.*, 2005), depending on the nature and thickness of the thermal insulator or pressure medium, as diamond has very high thermal conductivity. It should also be noted that the high thermal conductivity of diamond makes it difficult to maintain high temperatures greater than ~2000 K at pressures of the Earth's core ($P > 300$ GPa) in LHDAC, as the thickness of the thermal insulator becomes so thin that the sample cannot be efficiently heated by laser.

2.03.2.2 *Ab Initio* Calculation

Ab initio approaches are those that solve the fundamental equations of quantum mechanics with a bare minimum of approximations. DFT is, in principle, an exact theory for the ground state and allows us to reduce the interacting many-electron problem to a single-electron problem (the nuclei being treated as an adiabatic background). A key to the application of DFT in handling the interacting electron gas was given by Kohn and Sham (1965) by splitting the kinetic energy of a system of interacting electrons into the kinetic energy of noninteracting electrons plus some remainder, which can be conveniently incorporated into the exchange-correlation energy.

The local density approximation (LDA) replaces the exchange-correlation potential at each point by that of a homogeneous electron gas with a density equal to the local density at the point. The LDA works remarkably well for a wide variety of materials, especially in the calculations of EoS's, elastic constants, and other properties of silicates. Cell parameters and bulk moduli obtained from well-converged calculations often agree with the experimental data within a few percent and ~10%, respectively. Agreement with the laboratory data is not perfect, however, and some systematic discrepancies are noted for some materials.

Attempts to improve LDA via introducing nonlocal corrections have yielded some success. The generalized gradient approximation (GGA; Perdew *et al.*, 1992, 1996) is a significantly improved method over LDA for certain transition metals (Bagno *et al.*, 1989) and hydrogen-bonded systems (Hamann, 1997; Tsuchiya *et al.*, 2002, 2005a). There is some evidence, however, that GGA improves the energetics of silicates and oxides but the structures can be underbound. The volume and bulk modulus calculated with GGA tend to be larger and smaller, respectively, than those measured experimentally (Hamann, 1996; Demuth *et al.*, 1999; Tsuchiya and Kawamura, 2001). Considering the thermal effect with zero-point motion, LDA provides the structural and elastic quantities much closer (typically within a few percent) to experimental values than those obtained with GGA. In addition, a discrepancy of about $10 \sim 15$ GPa is usually seen in transition pressures calculated with LDA and GGA (Hamann, 1996; Tsuchiya *et al.*, 2004a, 2004c), which provide lower and upper bounds, respectively. Experimental transition pressures are usually found between the values obtained with LDA and GGA, although GGA tends to provide the pressure with better fit to the experimental value than LDA (Hamann, 1996; Tsuchiya *et al.*, 2004a, 2004c). The main source of computational error can be attributed to how to treat the exchange-correlation potential.

The standard DFT has limitations in applying to Fe-bearing oxides and silicates in the following case. One-electron approximation with the standard DFT approaches fails to describe the electronic structure of Fe–O bonding correctly due to its strongly correlated behavior. Both LDA and GGA usually produce metallic bands for Fe–O bonding in silicates. They also do not provide the correct crystal field effects that break the d-orbital degeneracy. More sophisticated classes of technique, such as LDA + U, LDA + DMFT (dynamical mean-field theory), multireference configurational interaction, etc., are needed to treat the many-body effect of electrons more accurately and to investigate geophysically important iron-bearing systems.

Among these schemes, LDA + U (Anisimov *et al.*, 1991) is the most practical method for minerals under the current state of computer technology. The main problem of applying LDA + U to materials under pressure is the determination of the effective

Hubbard U parameter, meaning screened on-site Coulomb interaction. Tsuchiya *et al.* (2006) computed the effective U in magnesiowüstite $(Mg_{1-x}Fe_x)O$ in a nonempirical and internally consistent way based on a linear response approach for the occupancy matrix (Cococcioni and de Gironcoli, 2005). Thus, the *ab initio* LDA + U technique appears to open a new way to explore the mineral physics properties of iron-bearing systems relevant to the Earth's deep interior (*see* Chapter 2.13).

2.03.2.3 Pressure Scale

The construction of an accurate pressure standard is a critical issue in the quantitative measurements of mineral physics properties under high pressure. The pressure (P)–volume (V)–temperature (T) equation of state (PVT-EoS) of materials is most useful in evaluating the experimental pressures under the P,T conditions of the Earth's deep mantle. The EoS of a pressure standard is usually derived on the basis of a conversion of dynamical shock Hugoniot data to isothermal compression data. In principle, some parameters specifying the thermal properties of a solid are necessary for this conversion process of the Hugoniot. However, measurements of these parameters without any pressure and also temperature standards are virtually impossible. In all EoS's presently used as primary pressure standards, the conversion of the Hugoniot was therefore performed with some simple assumptions about the unknown high-pressure behavior of the conversion parameters. The most critical issue on the validity of such assumptions is the volume dependence of the thermodynamic Grüneisen parameter, which is a fundamental quantity characterizing the thermal effect on the material.

The characteristic properties of gold (Au), namely its low rigidity, simple crystal structure, chemical inertness, and structural stability, make it particularly suitable as a pressure standard under high P,T conditions, and it has therefore been used as a primary standard in many *in situ* X-ray diffraction studies (e.g., Mao *et al.*, 1991; Funamori *et al.*, 1996). However, some recent *in situ* experiments noted that the pressure values estimated by different thermal EoS's of gold show significant discrepancies. Using the EoS of gold proposed by Anderson *et al.* (1989), which is frequently used as the pressure scale in experiments using multianvil apparatus, Irifune *et al.* (1998a) first reported that the postspinel phase boundary of Mg_2SiO_4 shifted to about 2.5 GPa lower than the pressure corresponding to the depth of the 660 km seismic discontinuity (~23.5 GPa and ~2000 K). Similar results were obtained for other various minerals as summarized in Irifune (2002).

Tsuchiya (2003) predicted the thermal properties and the PVT-EoS of gold based on the *ab initio* theory including thermal effect of electrons. The state-of-the-art *ab initio* calculation showed that the relationship $\gamma/\gamma_0 = (V/V_0)^q$, assumed in some studies, is adequate for gold, at least up to $V/V_0 = 0.7$ and the predicted value of q was 2.15, which is intermediate between the values used in Heinz and Jeanloz (1984) and Anderson *et al.* (1989). According to this study, the *ab initio* EoS model reduced the discrepancies between the observed phase boundaries of spinel, ilmenite, and garnet, and the seismic discontinuity. However, a gap of about 0.7 GPa still remains between the postspinel transition pressure and that of the 660 km discontinuity. The similar conclusions with a slightly larger (1.0–1.4 GPa) discrepancy have also been obtained by an experimental study using an empirical PVT-EoS model of MgO to determine pressure (Matsui and Nishiyama, 2002).

Even for gold, there are several PVT models derived by different groups, which are still not mutually consistent. Such a problem is also found in EoS's of platinum (Jamieson *et al.*, 1982; Holmes *et al.*, 1989). Moreover, platinum appears to be unsuitable for the pressure scale in some cases, because of its reactivity with the sample or materials of the experimental cell at high P,T conditions (Ono *et al.*, 2005a). A similar problem is also encountered with the pressures obtained using MgO. The pressures obtained using EoS's of different materials therefore show a significant scatter. Akahama *et al.* (2002) determined the pressures based on room-temperature EoS's of several materials compressed simultaneously in a diamond-anvil cell and reported that the EoS of platinum proposed by Holmes *et al.* (1989) provided pressures more than 10 GPa higher than those calculated using EoS of gold as proposed by Anderson *et al.* (1989) at pressures of a megabar even at 300 K. A similar inconsistency has also been reported in pressure determination based on gold and silver EoS's (Akahama *et al.*, 2004).

Examples of the difference in pressures based on different EoS's of gold and platinum are shown in **Figure 1**, along a temperature (2300 K) close to the typical lower-mantle geotherm. The pressures evaluated based on various EoS's of gold differ by ~2–3 GPa at the pressures of the uppermost parts of the lower mantle (25–30 GPa), and are within

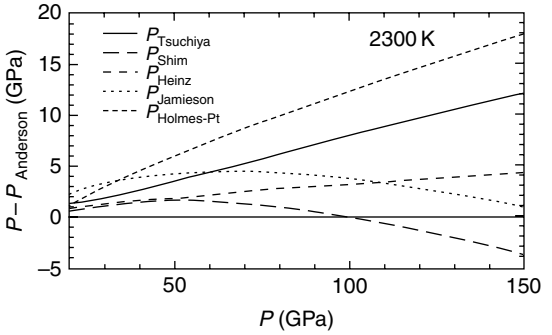

Figure 1 Differences between the pressures calculated using various EoS's of gold (Tsuchiya, 2003; Shim *et al*., 2002a; Heinz and Jeanloz, 1984; Jamieson *et al*., 1982) and those based on Anderson *et al*. (1989, horizontal line) as a function of pressure at 2300 K. The difference between the pressures using the Anderson scale and those using EoS of platinum by Holmes *et al*. (1989) is also shown for comparison.

5 GPa at pressures up to ~60 GPa. However, the differences become substantially larger at higher pressures, reaching ~15 GPa at the base of the lower mantle (136 GPa). It is also seen that the pressures based on an EoS of Pt (Holmes *et al*., 1989) are even higher than the highest pressure estimation by Tsuchiya (2003) by 5 GPa at 136 GPa. Thus the establishment of the mutually consistent pressure scales is urgently needed for more accurate experimental evaluation of phase transition and mineral physics under the lower-mantle P,T conditions.

2.03.3 Mineral-Phase Transitions in the Lower Mantle

2.03.3.1 Major Minerals in the Mantle and Subducted Slab

Phase transitions in Earth-forming materials dominate the structure and dynamics of the Earth. Major changes in seismic velocities traveling through the Earth's mantle can be generally attributed to the phase transitions of the constituent minerals, although some of them may be closely related to some chemical changes. Exploration and investigation of high-pressure phase transitions in mantle minerals have therefore been one of the major issues in studying the Earth's deep interior.

Here, we summarize the phase transitions in major minerals under lower-mantle conditions. Phase transitions in some relatively minor minerals relevant to the subducted slab lithologies are also reviewed in the following section. As the experimental data on the phase transitions are still limited and controversial at P,T conditions of the lower mantle, we have tried to construct the most likely phase diagrams for the minerals with simple chemical compositions based on available laboratory data and *ab initio* calculations. Thermoelastic properties of some key high-pressure phases are also reviewed and summarized here, as far as experimental data or theoretical predictions are available.

2.03.3.1.1 $MgSiO_3$

The high-pressure orthorhombic perovskite polymorph of $MgSiO_3$ (Mg-Pv) is believed to be the most abundant mineral in the Earth's lower mantle. The possibility of a further phase transition of this phase under the lower-mantle P,T conditions has been controversial. Some studies suggested that Mg-Pv dissociates into an assemblage of SiO_2 and MgO at 70–80 GPa and 3000 K (Meade *et al*., 1995; Saxena *et al*., 1996) or that it undergoes a subtle phase change above 83 GPa and 1700 K (Shim *et al*., 2001b), while others claimed that Mg-Pv is stable almost throughout the lower mantle (e.g., Fiquet *et al*., 2000). However, more recent studies suggested that the result of Shim *et al*. (2001b) were due to misidentification of the diffraction peaks of a newly formed platinum carbide (Ono *et al*., 2005a). The dissociation of Mg-Pv into the oxides is also unlikely to occur in the Earth's mantle according to the subsequent experimental (Murakami *et al*., 2004a, 2005; Oganov and Ono, 2004) studies. Theoretical investigations also suggest that the dissociation should occur at extremely high pressure above 1 TPa (Umemoto *et al*., 2006).

Recently, the Pv to postperovskite (PPv) transition in $MgSiO_3$ was found to occur by *in situ* X-ray diffraction experiment using LHDAC and *ab initio* calculations at ~2500 K and ~125 GPa (Murakami *et al*., 2004a; Tsuchiya *et al*., 2004a; Oganov and Ono, 2004) (**Figure 2**), close to the P–T conditions of the D″ layer near the core–mantle boundary (CMB). The Mg-PPv phase has a crystal structure identical to that of $CaIrO_3$ with a space group *Cmcm*. This structure consists of silica layers stacking along the *b*-direction and intercalated Mg ions. In the silica layers, SiO_6 octahedra connect sharing edges along the *a*-direction and sharing corners along the *c*-direction. Thus, this structure is more favorable at high pressure than the Pv structure, although the cation coordinations are basically same in both structures.

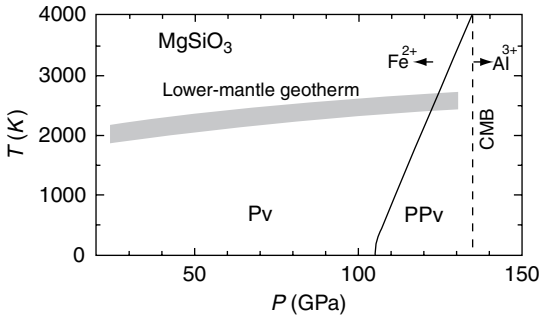

Figure 2 High *P*,*T* phase diagram for $MgSiO_3$ at lower-mantle pressures summarized based on the LHDAC experiments by Murakami *et al*. (2004a) and *ab initio* calculations by Tsuchiya *et al*. (2004a). Shaded area represents a typical lower-mantle geotherm based on Brown and Shankland (1981). Pv, perovskite; PPv, postperovskite; CMB, core–mantle boundary.

The PPv structure is expected to be highly anisotropic. It is more compressible along the *b*-direction perpendicular to the silica layers because only ionic Mg–O bonding exists in the interlayer spacing. The Pv and PPv structures therefore look very different in this respect. However, the structural relationship between Pv and PPv is quite simple and by applying shear strain ε_6, Pv can change to PPv directly (Tsuchiya *et al*., 2004a). According to this relation, the *c*-direction remains unchanged via the structural transition. This suggests that nonhydrostaticity could significantly affect the transition kinetics of the Pv-to-PPv transition.

PPv's thermodynamic properties and the position and slope of the phase boundary were investigated by means of *ab initio* quasiharmonic free energy calculations (Tsuchiya *et al*., 2004a, 2005b). The predicted Clapeyron slope of the Pv–PPv transition was $\sim 7.5\,\mathrm{MPa\,K^{-1}}$, which is remarkably close to that required for a solid–solid transition to account for the D″ discontinuity (Sidorin *et al*., 1999). Thus the results of both experimental and theoretical studies suggest that the PPv should be the most abundant high-pressure phase in the D″ region.

Over the past decades, there have been a number of experiments to determine elastic property of Mg-Pv (*e.g*., Yagi *et al*., 1982; Mao *et al*., 1991; Yeganeh-Haeri *et al*., 1989; Ross and Hazen, 1990; Funamori *et al*., 1996; Fiquet *et al*., 2000). Among these experiments, early studies yielded relatively large variations for zero-pressure bulk modulus K_0 of Mg-Pv ranging from 254 GPa (Ross and Hazen, 1990) to 273 GPa (Mao *et al*., 1991). However, more recent experiments of static compression and Brillouin spectroscopy yielded mutually consistent K_0 values of ~253–264 GPa. Density functional calculations have reported similar but slightly smaller room-temperature bulk modulus for Mg-Pv of about 250 GPa (Wentzcovitch *et al*., 2004; Tsuchiya *et al*., 2004b, 2005b). This underbinding tendency for Mg-Pv is seen in standard density functional calculations but is much more prominent in GGA than in LDA (Wentzcovitch *et al*., 2004).

In contrast to the extensive investigations of the EoS of Mg-Pv, the EoS of Mg-PPv has not been well constrained experimentally. According to a density functional prediction, the zero-pressure volume of Mg-PPv is very close to that of Mg-Pv (Tsuchiya *et al*., 2004a, 2005b). However, K_0 and its pressure derivative of Mg-PPv are significantly smaller and larger than those of Mg-Pv, respectively, which implies the volume of Mg-PPv should be smaller than that of Mg-Pv at the relevant pressure range. The volume decrease associated with the Pv–PPv transition is estimated to be ~1.5% on the basis of *ab initio* calculations (Tsuchiya *et al*., 2004a), which is consistent with those estimated based on LHDAC experiments.

2.03.3.1.2 $MgSiO_3$–$FeSiO_3$

Mg-Pv is supposed to incorporate 5–10 mol.% of $FeSiO_3$ in peridotitic compositions in the lower mantle (Irifune, 1994; Wood and Rubie, 1996; Katsura and Ito, 1996). However, experimental studies for the system $MgSiO_3$–$FeSiO_3$ have been limited to the pressures of the uppermost part of the lower mantle, except for an LHDAC study (Mao *et al*., 1991). Recent developments in KMA with sintered diamond anvils substantially extend the pressure and temperature ranges for phase equilibrium studies (as reviewed earlier), and Tange (2006) extensively studied the phase relations and the Mg–Fe partitioning between coexisting Mg-Pv and magnesiowüstite (Mw) at pressures up to ~50 GPa and temperatures to 2300 K.

Immediately after the discovery of the Pv–PPv transition in $MgSiO_3$, the effects of iron on this transition were studied using LHDAC (Mao *et al*., 2004, 2005). It was noted that the presence of iron significantly reduces the stability pressure of PPv, and PPv with up to ~80 mol.% of the $FeSiO_3$ component was synthesized at a pressure of ~140 GPa and at temperatures of ~2000 K (Mao *et al*., 2005). Thus the phase relations in the system $MgSiO_3$–$FeSiO_3$ at pressure up to ~130 GPa and at a typical lower-mantle temperature can be drawn as illustrated in **Figure 3**, according to the results of these and

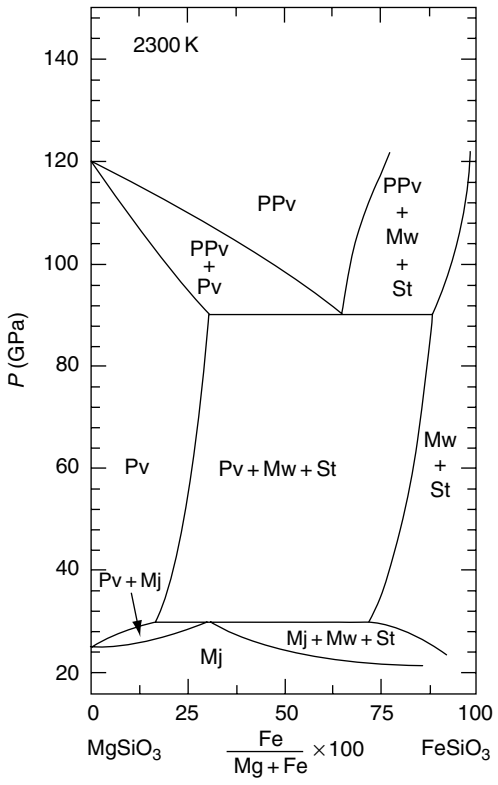

Figure 3 A predicted phase diagram for the system $MgSiO_3$–$FeSiO_3$ at lower-mantle pressures and at a representative lower-mantle temperature (2300 K). The relations below ~30 GPa are estimated on the basis of Sawamoto (1987) and Ohtani *et al*. (1991) using KMA, while those above 80 GPa are based on LHDAC experiments by Mao *et al*. (2004, 2005). The boundaries between these pressures are depicted based on recent experimental data using KMA with SD anvils (Tange, 2006). Mj, majorite garnet; Mw, magnesiowüstite; St, stishovite.

Tange's studies. Although a significant effect of ferrous iron on the stability of Mg-PPv has been predicted by some theoretical works using GGA (Caracas and Cohen, 2005b; Stackhouse *et al*., 2006), the latest experiment showed much smaller effects (Sinmyo *et al*., 2006). Nevertheless, this issue has not been fully resolved yet and there remains large room for further theoretical and experimental investigations.

Effect of iron on the PPv transition has also been studied in the light of the high-pressure phase changes of hematite, corundum-type Fe_2O_3. Hematite transforms first to the high-pressure phase with the *Pbnm* Pv structure or Rh_2O_3(II) structures at 30 GPa, whose X-ray diffraction patterns are very similar to each other (Ono *et al*., 2005b). Further transitions in Fe_2O_3 to the structure assigned as the $CaIrO_3$-type structure has been reported to occur at a transition pressure of ~50 GPa (Ono *et al*., 2005b). This transition pressure is significantly lower than the Pv–PPv transition pressure in $MgSiO_3$. Thus the presence of iron in the trivalent state is also suggested to lower the pressure of the Pv–PPv transition, as is found for divalent iron.

2.03.3.1.3 $MgSiO_3$–Al_2O_3

Irifune (1994) demonstrated that Mg-Pv is the major host of aluminum in a pyrolite composition at pressures and temperatures of the uppermost parts of the lower mantle, possessing ~4 mol.% of Al_2O_3. Phase relations in the system $MgSiO_3$–Al_2O_3 under the lower-mantle conditions have since been studied (Irifune *et al*., 1996a; Ito *et al*., 1998) with an emphasis on the $MgSiO_3$–$Mg_3Al_2Si_3O_{12}$ system. Irifune *et al*. (1996a) showed that majorite garnet with less than ~15 mol.% Al_2O_3 transforms to the Pv structure via a mixture of these two phases, while this assemblage further changes to an assemblage of majorite plus corundum at pressures about ~28 GPa, at 1800 K. This assemblage with the $Mg_3Al_2Si_3O_{12}$ composition was later shown to form almost pure Pv at ~38 GPa using KMA with SD anvils (Ito *et al*., 1998).

Phase transitions in Al_2O_3 corundum under the lower-mantle condition were first studied by Funamori and Jeanloz (1997) using LHDAC based on earlier *ab initio* predictions (Marton and Cohen, 1994; Thomson *et al*., 1996), which demonstrated that corundum transforms to a new phase with the Rh_2O_3(II) structure at ~100 GPa and at ~1000 K. More recently, it has been predicted by *ab initio* studies that Al_2O_3 has a similar high-pressure phase relation to Fe_2O_3 (Caracas and Cohen, 2005a; Tsuchiya *et al*., 2005c; Stackhouse *et al*., 2005b). The Pv-to-PPv transition was thus suggested to occur in Al_2O_3 at about 110 GPa at 0 K, although the Pv phase is eclipsed by the stability field of the Rh_2O_3(II) phase. This Pv-to-PPv transition pressure in Al_2O_3 is about 10 GPa higher but fairly close to that in $MgSiO_3$, though Akber-Knutson *et al*. (2005) predicted a much larger effect of Al by estimating the solid solution energy. *In situ* X-ray diffraction experiments on pyrope compositions by LHDAC (Tateno *et al*., 2005) demonstrated a consistent result about the effect of aluminum incorporation on the PPv transition pressure. Therefore, we expect that though aluminum tends to increase the PPv transition pressure in $MgSiO_3$, the effect is not very significant. The plausible phase diagram of the system $MgSiO_3$–Al_2O_3 in the lower-mantle P,T condition is illustrated in **Figure 4**.

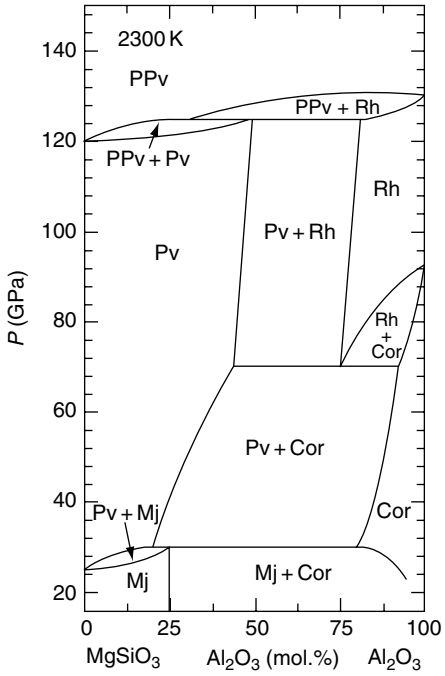

Figure 4 A predicted phase diagram for the system $MgSiO_3$-Al_2O_3 at lower mantle pressures and at 2300K. The phase relations below ~40 GPa are based on KMA experiments (Irifune *et al*., 1996a; Ito *et al*., 1998), while those on Al_2O_3 are from Funamori *et al*. (1998) using LHDAC and *ab initio* calculations by Tsuchiya *et al*. (2005c). The results of Tateno *et al*. (2005) and Tsuchiya *et al*. (2005c) were also taken into account to illustrate the phase relations at 120-130 GPa. Cor, corundum; Rh, Rh_2O_3(II).

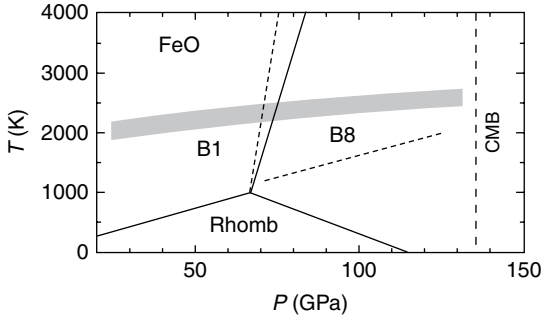

Figure 5 High *P*,*T* phase diagram for FeO at lower-mantle pressures summarized based on the *in situ* measurement by Fei and Mao (1994), Murakami *et al*. (2004b), and Kondo *et al*. (2004). B1, NaCl structure; B8, NiAs structure; Rhomb, rhombohedral B1 phase.

2.03.3.1.4 MgO–FeO

Mw, $(Mg_{1-x}Fe_x)O$, is believed to be the next major mineral phase in Earth's lower mantle after ferrosilicate Pv, $(Mg_{1-x}Fe_x)SiO_3$ (e.g., Helffrich and Wood, 2001). The magnesium end member of Mw, periclase, possessing the B1 (NaCl) structure is known to be an extraordinarily stable phase. No phase transitions in this material have been observed or predicted under the *P*,*T* conditions of the entire mantle (Duffy *et al*., 1995; Alfé *et al*., 2005), primarily due to substantially smaller ionic radius of magnesium relative to that of oxygen. FeO wüstite, on the other hand, transforms to an antiferromagnetic phase accompanied by a small rhombohedral distortion. This transition is a typical magnetic order–disorder transition and therefore the transition temperature corresponds to the Neel point. Although the rhombohedral B1 (rB1) phase is stable at low temperatures up to about 110 GPa, at higher pressure over 65 GPa and high temperatures, the rB1 phase transforms to the normal or inverse B8 (NiAs) structure, as shown in **Figure 5** (Fei and Mao, 1994; Murakami *et al*., 2004b; Kondo *et al*., 2004). However, several important properties of this high-pressure phase such as high-temperature stability, structural details, and electronic property are still in debate (Fei and Mao, 1994; Mazin *et al*., 1998; Murakami *et al*., 2004b).

For the compositions between these two end members, some controversial experimental results have emerged: Mw with $X_{Fe} = 50\%$ was reported to dissociate into two components, Fe-rich and Mg-rich Mw's at 86 GPa and 1000 K (Dubrovinsky *et al*., 2000). In contrast, another study using LHDAC found no dissociation of Mw with even higher X_{Fe} of 0.61 and 0.75 up to 102 GPa and 2550 K, though the sample with $X_{Fe} = 0.75$ showed a displacive transition to the rB1 structure at low temperature similar to FeO wüstite (Lin *et al*., 2003). Thus, further experimental and theoretical studies are required to address the possible dissociation of Mw.

Another issue relevant to Mw, as well as the ferrosilicate Pv, which should affect thermoelastic properties of these phases, is the occurrence of electron spin transitions under the lower-mantle conditions. High spin (HS) to low spin (LS) transitions in iron have been observed by *in situ* X-ray emission spectroscopy (XES) and Mössbauer spectroscopy from 40 to 70 GPa in Mw containing about 18% of iron (Badro *et al*., 2003; Lin *et al*., 2005) and from 70 and 120 GPa in $(Mg,Fe)SiO_3$ Pv (Badro *et al*., 2004; Li *et al*., 2004; Jackson *et al*., 2005) at room temperature. Several significant effects on thermochemical state of the lower mantle can be inferred by the spin transition of iron. The spin transition in Mw is accompanied by significant volume reductions (Lin *et al*., 2005; Tsuchiya *et al*., 2006) and changes in these

minerals' optical absorption spectrum (Badro *et al.*, 2004). These can produce (1) seismic velocity anomalies, (2) variations in $Mg-Fe^{2+}$ partitioning between Mw and Pv, (3) changes in radiative heat conductivity, and (4) compositional layering (Gaffney and Anderson, 1973; Badro *et al.*, 2003, 2004). The elastic signature of this transition in Mw has been partially explored (Lin *et al.*, 2005), but there is still much uncertainty. In contrast, anomalous compression behavior has not yet been observed in $(Mg,Fe)SiO_3$ Pv.

The strongly correlated behaviour of iron oxide has deterred the quantification of these changes by density functional calculations based on the local spin density (LSDA) and spin polarized generalized gradient approximations (σ-GGA). These approaches incorrectly predict a metallic HS ground state and then successive spin collapses across the transition as reported for FeO (Sherman and Jansen, 1995; Cohen *et al.*, 1997). More recently, a new model explaining the mechanism of HS-to-LS transition of iron in Mw has been proposed based on calculations using more sophisticated LDA + U technique that describe the electronic structure of strongly correlated system more correctly (Tsuchiya *et al.*, 2006). In this study, the effective Hubbard U parameter has been optimized at each volume and at each iron concentration up to X_{Fe} of 18.75% in an internally consistent way. As a result, it has been demonstrated that the large stability field of HS/LS mixed state appears at high temperatures instead of the intermediate spin state, due to the contributions of coexisting HS/LS mixing entropy and magnetic entropy. According to this transition mechanism, Mw is expected to be in this HS/LS mixed state for almost the entire range of lower-mantle *P*,*T* conditions, with the proportion of HS iron decreasing continuously with increasing pressure (**Figure 6**). No discontinuous change in any physical properties would appear associated with the spin transition in Mw within this range.

It has been reported that the spin transition pressure significantly increases with increasing X_{Fe}. A volume decrease associated with the spin transition was observed in $(Mg_{0.4}Fe_{0.6})O$ at 95 GPa (Lin *et al.*, 2005), while no spin transition has so far been reported in pure FeO up to 143 GPa (Badro *et al.*, 1999). Iron–iron interactions, which are no longer negligible at X_{Fe} higher than 20%, might also reinforce the magnetic moment significantly, although the mechanism of this tendency has not been fully understood to date.

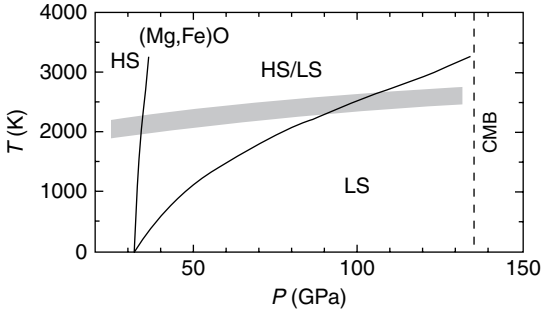

Figure 6 High *P*,*T* spin transition diagram for Mw with iron concentration of 18.75% at lower-mantle pressures predicted on the basis of LDA + U calculations by Tsuchiya *et al*. (2006). HS, high spin; LS, low spin.

2.03.3.1.5 $CaSiO_3$

The lower mantle is believed to consist mainly of $(Mg,Fe)SiO_3$ Pv and Mw, with some $CaSiO_3$ perovskite (Ca-Pv) up to 7–8 vol.% (e.g., Irifune, 1994). Despite its importance, there are many unanswered questions about the structure, stability, the EoS, and other physical properties of Ca-Pv under pressure and temperature, which complicate some attempts to model the mineralogy of the lower mantle (Stacey and Isaak, 2001).

$CaSiO_3$ crystallize to the Pv structure over 10–13 GPa, depending on temperature, and is known to be unquenchable at ambient conditions. At lower-mantle conditions, $CaSiO_3$ has an ideal cubic Pv structure, while at lower temperatures it is suggested to be slightly distorted. The small degree of the possible distortion is hardly observed by current high-temperature and high-pressure X-ray techniques, and several orthorhombic and tetragonal structures have been proposed, based on *in situ* X-ray diffraction measurements (Shim *et al.*, 2002b; Kurashina *et al.*, 2004; Ono *et al.* 2004) or theoretical calculations (Stixrude *et al.*, 1996; Chizmeshya *et al.*, 1996; Magyari-Köpe *et al.*, 2002; Caracas *et al.*, 2005).

EoS of Ca-Pv has been determined up to CMB pressures by different groups (e.g., Mao *et al.*, 1989; Tamai and Yagi, 1989; Wang *et al.*, 1996; Shim *et al.*, 2000a, 2000b, 2002b; Kurashina *et al.*, 2004; Ono *et al.*, 2004; Shieh *et al.*, 2004). The fitting of the experimental results by third-order Birch–Murnaghan EoS, yielded a unit-cell volume, $V_0 = 45.54$ Å^3, bulk modulus, K_0, ranging from 232 to 288 GPa, and its pressure derivative, K_0', within 3.9–4.5. Most of the recent results with careful removing of the effect of deviatoric stress on the produced pressure, however, yielded the lower end values (232–236 GPa; Wang

et al., 1996; Shim *et al.*, 2000b) in this range. The results of corresponding *ab initio* studies (e.g., Wentzcovitch *et al.*, 1995; Chizmeshya *et al.*, 1996; Stixrude *et al.*, 1996; Karki and Crain, 1998) are similar to those obtained for the experimental data. Most of these studies, both experimental and theoretical, have focused on the behavior of the cubic modification of $CaSiO_3$ under pressure.

Caracas *et al.* (2005) performed a detailed investigation of the major symmetry-allowed modifications of $CaSiO_3$ obtained as distortions from the parent cubic phase by means of *ab initio* pseudopotential theory. They examined nine modifications having different symmetries and reported that the I4/mcm phase is the most likely stable static atomic configuration up to about 165 GPa. Enthalpy difference between this I4/mcm and the cubic Pv phase increased with increasing pressure, indicating that the I4/mcm structure becomes more stable relative to the cubic structure at higher pressure. The bulk modulus was estimated to be about 250 GPa for all modifications with the exception of R-3c structure. This theoretical K_0 is fairly similar to recent experimental values (Wang *et al.*, 1996; Shim *et al.*, 2002b), but much smaller than those reported in earlier nonhydrostatic experiments (Mao *et al.*, 1989; Tamai and Yagi, 1989).

Some studies focused on the high-temperature phase change from low symmetry phase to cubic Ca-Pv. Ono *et al.* (2004) reported that this transition occurs at about 600–1200 K at 25–120 GPa, where the transition temperature increased with increasing pressure, consistent with the theoretical prediction (Caracas *et al.*, 2005). These temperatures are much lower than the typical lower-mantle geotherm of about 2000–2500 K, suggesting that $CaSiO_3$ may have the cubic form throughout the actual lower mantle (**Figure 7**). However, most recent *ab initio* molecular dynamics studies (Li *et al.*, 2006a, 2006b) reported very different results. They found the tetragonal phase stable even at the mantle temperatures in addition to the low-temperature stability of the orthorhombic phase. Their calculated elasticity of Ca-Pv is also very different from earlier results (Karki and Crain, 1998), particularly with respect to the shear modulus. The cause of the discrepancies is unclear.

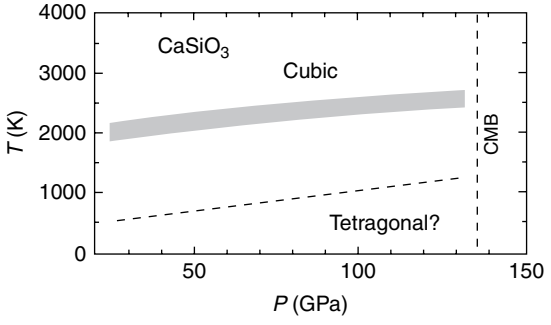

Figure 7 High *P*,*T* phase diagram for $CaSiO_3$ at lower-mantle pressures summarized based on the LHDAC experiments by Kurashina *et al*. (2004) and Ono *et al*. (2004).

2.03.3.1.6 SiO_2

Recent theoretical studies suggested that a second-order displacive phase transition from stishovite to the $CaCl_2$-type structure occurs at 50–60 GPa at room temperature (Kingma *et al.*, 1995). It has also been predicted that the $CaCl_2$-type silica undergoes a further structural transition to the α-PbO_2 phase (Dubrovinsky *et al.*, 1997; Karki *et al.*, 1997a). The results of the experimental studies on these issues, however, have been controversial. LHDAC studies reported that the $CaCl_2$-type phase persists at least up to 120 GPa (Andrault *et al.*, 1998), and the transition to the α-PbO_2 phase occurs at 121 GPa and 2400 K (Murakami *et al.*, 2003). In contrast, another similar experiment showed that the α-PbO_2-like phase was formed from cristobalite above 37 GPa at room temperature, and that stishovite directly transformed to the α-PbO_2-type structure above 64 GPa at 2500 K with a negative Clapeyron slope (Dubrovinsky *et al.*, 2001). In addition, Sharp *et al.* (1999) found the α-PbO_2-type phase in a natural meteorite sample, which would have experienced very low shock pressure below 30 GPa. These discrepancies may come from various difficulties in LHDAC experiments, such as associated with kinetic problems, temperature or pressure uncertainties, effect of different starting materials, etc.

During the last decade, a series of theoretical studies (Kingma *et al.*, 1995; Dubrovinsky *et al.*, 1997; Karki *et al.*, 1997a) also addressed this issue of the post-stishovite phase transitions in the framework of the *ab initio* calculations. These early theoretical studies were limited to static conditions, the calculations being performed at $T = 0$ K, without considering the zero-point energy. To investigate the contradictory experimental results on the high-temperature phase stability of SiO_2 under high pressure, finite temperature thermal effect on the transitions obtained by these static calculations should be taken into account.

Tsuchiya *et al.* (2004c) predicted the high-pressure and high-temperature phase equilibrium of

three ordered modifications of SiO_2 using *ab initio* density functional perturbation theory and the quasiharmonic approximation. The predicted stishovite-$CaCl_2$ phase transition boundary is $P = 56 + 0.0059T$ (K) GPa, which is consistent with the results of LHDAC experiment by Ono *et al.* (2002). This predicted slope of the stishovite–$CaCl_2$ boundary of about $5.9\,MPa\,K^{-1}$ is close to but slightly larger than the earlier rough estimate of $4\,MPa\,K^{-1}$ (Kingma *et al.*, 1995). The LHDAC experiment resulting in a stishovite–α-PbO_2 boundary with a negative Clapeyron slope (Dubrovinsky *et al.*, 2001), which disagrees with the phase diagram based on Tsuchiya *et al.* (2004c), as shown in **Figure 8**. This disagreement may be due to experimental uncertainties and/or to kinetic problems in the former LHDAC experiment. These are supported by later calculations by Oganov *et al.* (2005), though they proposed substantially lower transition pressures primarily due to the application of LDA (see Section 2.03.2.2).

On the other hand, the phase transition boundary between $CaCl_2$ and α-PbO_2 in SiO_2 is predicted to be $P = 106.3 + 0.005\,79T$ (K) GPa based on *ab initio* calculations (Tsuchiya *et al.*, 2004c), which locates near the lowermost-mantle P,T conditions. This calculation also indicates that the α-PbO_2-type phase is the stable form of silica at depths down to the CMB, consistent with the result of an LHDAC experiment (Murakami *et al.*, 2003). These theoretical and experimental results also suggest that the α-PbO_2-type phase silica recently discovered in the meteorite sample might have been formed by a metastable reaction.

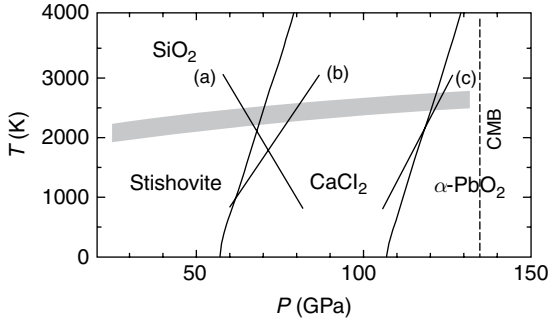

Figure 8 High P,T phase diagram for SiO_2 at lower-mantle pressures predicted by the *ab initio* calculations by Tsuchiya *et al*. (2004c). The results of *in situ* X-ray experiments using LHDAC by (a) Dubrovinsky *et al*. (2001), (b) Ono *et al*. (2002), and (c) Murakami *et al*. (2003) are also shown.

2.03.3.1.7 Al-rich phase

Majorite garnet is the main host of aluminum in the mantle transition region in both pyrolite and basaltic compositions. It transforms to an assemblage of Mg-Pv + Ca-Pv at pressures corresponding to the uppermost lower mantle. Aluminum is incorporated mostly in Mg-Pv in pyrolite composition (Irifune, 1994), whereas a separate aluminous phase is formed in basaltic compositions under the P,T conditions of the lower mantle, as demonstrated by Irifune and Ringwood (1993).

The aluminous phase, named as 'Al-rich phase' by these authors, was suggested to have a crystal structure similar to but not completely identical to the calcium ferrite structure. This Al-rich phase was later proposed to have a hexagonal structure or NAL-phase (Miyajima *et al.*, 2001; Akaogi *et al.*, 1999; Sanehira *et al.*, 2005), whereas others proposed that this phase possesses the calcium ferrite structure (Kesson *et al.*, 1998; Hirose *et al.*, 1999; Ono *et al.*, 2005d). Although the stability relations of these two phases in MORB compositions are not very clear to date, only very minor effects on the mineralogy and dynamics in the lower mantle is expected by the possible misidentification of these two phases under the lower-mantle conditions (Sanehira *et al.*, 2005; Shinmei *et al.*, 2005), as the crystal structures of these two phases are quite similar and yield only slight difference in densities.

2.03.3.2 Minor Minerals

2.03.3.2.1 $MgAl_2O_4$, $NaAlSiO_4$

$MgAl_2O_4$ spinel is known to decompose to simple oxides of MgO and Al_2O_3 at pressure and temperatures of mantle transition region, which recombine to form a calcium ferrite ($CaFe_2O_4$, CF) type phase at about 25 GPa (Irifune *et al.*, 1991; Funamori *et al.*, 1998; Akaogi *et al.*, 1999). Although the formation of an unknown phase named ε-phase (Liu, 1978) was reported at a similar pressure at 1300 K in LHDAC experiments, none of the subsequent LHDAC and KMA experiments using both quench and *in situ* X-ray measurements have confirmed this phase. Instead, it has been shown that the CF-phase further transforms to a calcium titanate ($CaTiO_4$, CT) phase at pressures of ~40–45 GPa (Funamori *et al.*, 1998). An *ab initio* periodic LCAO (linear combination of atomic orbitals) calculation by Catti (2001) demonstrated that the calcium titanate structure is indeed stable

relative to the calcium ferrite structure at pressures greater than ~39–57 GPa.

$NaAlSiO_4$ also adopts the calcium ferrite structure at pressures above 25 GPa (Liu, 1977; Akaogi *et al.*, 1999), but the formation of the complete solid solutions between this and $MgAl_2O_4$ has not been reported, as there is a region of the hexagonal phase in the intermediate region of these end-member compositions (Akaogi *et al.*, 1999; Shinmei *et al.*, 2005). It was demonstrated that the CF-type $NaAlSiO_4$ is stable at least at pressures up to 75 GPa and temperatures to 2500 K on the basis of LHDAC experiments (Tutti *et al.*, 2000).

2.03.3.2.2 $KAlSi_3O_8$, $NaAlSi_3O_8$

$KAlSi_3O_8$-rich feldspar, an important mineral in K-rich basalt (e.g., Wang and Takahashi, 1999) and continental crust and marine sediment lithologies (Irifune *et al.*, 1994), transforms to the hollandite structure via a mixture of $K_2Si_2O_5$ wadite + Al_2O_5 kyantite + SiO_2 coesite at about 9 GPa. $KAlSi_3O_8$ hollandite plays an important role in fractionation of some trace elements because of its peculiar tunnel structure that accommodates large ion lithophile elements (Irifune *et al.*, 1994). Although an LHDAC study suggested that this structure is stable almost throughout the lower-mantle P,T conditions (Tutti *et al.*, 2001), recent *in situ* X-ray diffraction studies using DAC with a helium pressure medium at room temperature (Ferroir *et al.*, 2006) and KMA at high pressure and high temperature demonstrated that the hollandite transforms to an unquenchable phase, named as hollandite II (Sueda *et al.*, 2004), at about 22 GPa at room temperature with a positive Clapeyron slope. Although only a slight modification in crystal structures between these phases was noted (Ferroir *et al.*, 2006), this transition may significantly affect partitioning of some trace elements between the K-hollandite and coexisting melts in the lower mantle.

$NaAlSi_3O_8$-rich hollandite was found in shock veins of some meteorites (e.g., Tomioka *et al.*, 2000; Gillet *et al.*, 2000). However, attempts to reproduce the hollandite with such compositions by high-pressure experiments have failed (Yagi *et al.*, 1994; Liu, 2006), as the solubility of this component is limited to about 50 mol.% at pressures of ~22 GPa and at temperatures up to 2500 K. Thus this phase could have been formed metastably in a very short period of time under shock compression in the parental bodies of these meteorites.

2.03.3.2.3 CAS phase

The 'CAS phase' was first described by Irifune *et al.* (1994) as a new Ca- and Al-rich high-pressure phase in a continental crust composition at pressures above ~15 GPa, which was suggested to be a major host for aluminum and calcium in the subducted marine sediments in the mantle transition region. Subsequent experimental studies demonstrated that this phase has the ideal composition of $CaAl_4Si_2O_{11}$, possessing a hexagonal barium ferrite-type structure with space group $P6_3/mmc$ (Gautron *et al.*, 1999). Moreover, this high-pressure phase with a composition of $(Ca_xNa_{1-x})Al_{3+x}Si_{3-x}O_{11}$ was recently discovered in a shergottite shocked Martian meteorite in association with stishovite and/or K, Na-rich hollandite (Beck *et al.*, 2004), both of which are known to be stable only at pressures above ~9 GPa.

The CAS phase is suggested to have silicon in fivefold coordination in a trigonal bipyramid site at high pressure and high temperature, which is supposed to decompose into fourfold and sixfold coordinations upon quenching and subsequent release of pressure (Gautron *et al.*, 1999). *In situ* Raman spectroscopy and X-ray diffraction measurements actually indicated the formation of fivefold coordinated silicon under pressure, which should play an important role in the transport properties of minerals through the formation of oxygen vacancies (Gautron *et al.*, 2005).

2.03.3.2.4 Phase D, δ-AlOOH

Phase D was first noted by Liu (1986) as a new dense hydrous magnesium (DHMS) phase in serpentine, which was later confirmed by *in situ* X-ray diffraction (Irifune *et al.*, 1996b). Both X-ray power diffraction profile and the chemical composition of this phase were also refined on the quenched sample (Irifune *et al.*, 1996b; Kuroda and Irifune, 1998). Two groups subsequently succeeded in refining its crystal structure independently (Yang *et al.*, 1997; Kudoh *et al.*, 1997). The stability of phase D has since been studied experimentally using both KMA (Ohtani *et al.*, 1997; Irifune *et al.*, 1998b; Frost and Fei, 1998) and LHDAC (Shieh *et al.*, 1998), which demonstrated that this phase has a wide stability field up to 40–50 GPa, at temperatures to ~1800 K, whereas it dehydrates to form an assembly containing Mg-Pv and Mw at higher temperatures (Shieh *et al.*, 1998).

Serpentine is the major hydrous mineral in the subducted slab, and phase D should be the only possible DHMS present in the upper part of the lower mantle transported via the subduction of slabs

(Irifune *et al.*, 1998b; Shieh *et al.*, 1998; Ohtani *et al.*, 2004), although the newly found δ-AlOOH (Suzuki *et al.*, 2000) could be an alternative water reservoir in the lower mantle under very limited Al-rich circumstances. For both phase D and δ-AlOOH, structural changes associated with hydrogen bond symmetrization are expected to occur on the basis of *ab initio* calculations (Tsuchiya *et al.*, 2002, 2005a), which should affect the compressional behavior and hence density changes of these hydrous phases in the lower mantle.

2.03.3.2.5 $MgCO_3$, $CaCO_3$

Carbonates are important constituents of pelagic sediments, parts of which are supposed to subduct into the mantle. It has been shown that $MgCO_3$ magnesite is the major carbonate in the mantle (e.g., Biellmann *et al.*, 1993), whose stability under high pressure has been studied using LHDAC. Magnesite was reported to be stable at pressures up to 80 GPa, almost throughout the lower mantle (Gillet, 1993, Fiquet *et al.*, 2002), but a recent *in situ* X-ray diffraction study demonstrated it transforms to an unknown phase (magnesite II) at pressures above ~115GPa, at 2000–3000 K (Isshiki *et al.*, 2004). Although the dissociation of magnesite into assemblages of $MgO + CO_2$ (Fiquet *et al.*, 2002) or $MgO + C + O_2$ (Liu, 1999) was suggested on the basis of thermodynamic considerations, such reactions are unlikely to occur along appropriate geotherms in the lower mantle (Isshiki *et al.*, 2004).

In contrast, certain amounts of $CaCO_3$ could survive in the subducted slabs without decarbonation or reaction with surrounding minerals, due to low temperatures of the slabs, and thus are delivered into the lower mantle. $CaCO_3$ adopts the aragonite structure under P,T conditions of the uppermost mantle, which was recently found to transform to a high-pressure form with an orthorhombic symmetry at pressures greater than ~40 GPa and at temperatures 1500–2500 K using LHDAC (Ono *et al.*, 2005c). Although the possibility of the transformation of $CaCO_3$ aragonite to a trigonal phase is suggested on the basis of DAC experiments at room temperature (Santillán and Williams, 2004), this phase could have been metastably formed, and the orthorhombic post-aragonite phase should be stable at least to depths of ~2000 km in the lower mantle (Ono *et al.*, 2005c). Thus, $MgCO_3$ and possibly $CaCO_3$ are the potential hosts of CO_2 throughout most parts of the lower mantle, except for the bottom parts of the D″ layer (Isshiki *et al.*, 2004).

2.03.4 Phase Transitions and Density Changes in Mantle and Slab Materials

2.03.4.1 Chemical Compositions and Density Calculations

Subducting oceanic lithosphere is modeled by layers of basaltic oceanic crust of ~6 km thickness, underlain by thicker layers (~50–100 km) of residual harzburgite and fertile lherzolite, which are covered with thin (~1 km) terrigeneous and/or pelagic sediments. Typical chemical compositions of these lithologies are listed in **Table 1**. Most parts of the sedimentary materials are believed to be trapped to form accretion terrains underneath island arcs upon subduction of slabs at ocean trenches, although geochemical evidence suggests that certain parts of such materials may be subducted deeper into the mantle (e.g., Loubet *et al.*, 1988). At least part of the bottom warmer lherzolite layer of a slab may also be assimilated to the surrounding mantle during subduction in the upper mantle and mantle transition region, and thus the slab approaching the 660 km seismic discontinuity can reasonably be modeled by a layered structure of basaltic and harzburgitic rocks (Ringwood and Irifune, 1988).

The chemical composition of the lower mantle has been a major controversial issue in the mineralogy of the Earth's interior. Some (e.g., Ringwood, 1962) believe peridotitic or pyrolitic materials are dominant in the whole mantle, while others (e.g., Liu, 1982; Anderson, 1989; Hart and Zindler, 1986) claim that more Si-rich chondritic materials should be representative for the composition of the lower mantle (**Table 1**). The difference is based on rather philosophical arguments on the origin and subsequent differentiation processes of the Earth, which are critically dependent on the models of condensation/evaporation processes of elements and compounds in the primordial solar system and the possible formation of deep magma ocean in the early stage of the formation of the Earth. As the elastic properties, particularly those related to shear moduli, of high-pressure phases have not been well documented under the pressure and temperature conditions of the lower mantle, it is hard to unambiguously evaluate the feasibility of these two alternative composition models in the light of mineral physics and seismological observations (e.g., Bina, 2003; Mattern *et al.*, 2005). Moreover, the knowledge of variation of temperature with depth is vital to address this issue, which also has not been well constrained in the lower mantle.

Table 1 Representative chemical compositions of lower mantle and those related to subducting slabs

	Lower mantle				
	Chondrite	**Pyrolite**	**Harzburgite**	**MORB**	**Continental crust**
SiO_2	53.8	44.5	43.6	50.4	66.0
TiO_2	0.2	0.2		0.6	0.5
Al_2O_3	3.8	4.3	0.7	16.1	15.2
Cr_2O_3	0.4	0.4	0.5		
FeO	3.5	8.6	7.8	7.7	4.5
MgO	35.1	38.0	46.4	10.5	2.2
CaO	2.8	3.5	0.5	13.1	4.2
Na_2O	0.3	0.4		1.9	3.9
K_2O		0.1		0.1	3.4

MORB, mid-ocean ridge basalt.
Chondrite, Liu (1982); pyrolite, Sun (1982); harzburgite, Michael and Bonatti (1985); MORB, Green *et al*. (1979); continental crust, Taylor and McLennan (1985).

Table 2 PVT-EoS parameters of lower-mantle phases determined from various experimental and theoretical data and their systematics

	Mg-Pv	**Fe-Pv**	**Al_2O_3-Pv**	**Mg-PPv**	**Ca-Pv**	**MgO**	**FeO**	**SiO_2 (St)**	**SiO_2 (α-PbO_2)**
V_0 ($cm^3\,mol^{-1}$)	24.45	25.48	24.77	24.6	27.45	11.36	12.06	14.02	13.81
B_0 (GPa)	257	281	232	226	236	158	152	314	325
B'	4.02	4.02	4.3	4.41	3.9	4.4	4.9	4.4	4.2
Θ_D (K)	1054	854	1020	1040	984	725	455	1044	1044
γ	1.48	1.48	1.48	1.55	1.53	1.52	1.28	1.34	1.34
q	1.2	1.2	1.2	1.2	1.5	1.5	1.5	2.4	2.4

Mg-Pv (Shim and Duffy, 2000; Fiquet *et al*., 2000; Sinogeikin *et al*., 2004; Tsuchiya *et al*., 2004a, 2005b), Fe-Pv (Jeanloz and Thompson, 1983; Parise *et al*., 1990; Mao *et al*., 1991; Kiefer *et al*., 2002), Al_2O_3-Pv (Thomson *et al*., 1996; Tsuchiya *et al*., 2005c), Mg-PPv (Tsuchiya *et al*., 2004a, 2005b), Ca-Pv (Wang *et al*., 1996; Shim *et al*., 2000b; Karki and Crain, 1998), MgO (Fiquet *et al*., 1999; Sinogeikin and Bass, 2000), FeO (Jackson *et al*., 1990; Jacobsen *et al*., 2002; systematics), SiO_2 (Ross *et al*., 1990; Andrault *et al*., 2003; Karki *et al*., 1997a; Tsuchiya *et al*., 2004c).
High-T Birch–Murnaghan equation was applied only for the hexagonal aluminous phase with parameters $V_0 = 110.07\,cm^3\,mol^{-1}$, $B_0 = 185.5$ GPa, $B' = 4$ (fix), $dB/dT = -0.016\,GPa\,K^{-1}$ and $\alpha_0 = 3.44 \times 10^{-5}\,K^{-1}$ (Sanehira *et al*., 2005).

Here, we assume the whole mantle is of a pyrolitic composition to address the phase transitions and associated density changes in the lower mantle, as there are significant variations in the chondritic/cosmochemical models and also because high-pressure experimental data on the latter compositions have been scarce to date. We also assume the major lithologies transported into the lower mantle via subduction of slabs are of mid-ocean ridge basalt (MORB) and harzburgite compositions. Phase transitions in MORB have been extensively studied down to the depths near the mantle–core boundary. In contrast, although virtually no experimental data exist on harzburgite compositions in this depth region, they can be reasonably estimated from those available on the high-pressure phases with simple chemical compositions, as harzburgitic compositions have a minor amount of Fe and only very small amounts of Ca, and Al, and are well approximated by the MgO (FeO)–SiO_2 system.

We calculated the density changes in pyrolite, harzburgite, and MORB compositions using available experimental data as follows. The densities of the individual high-pressure phases that appeared in these lithologies were calculated at given pressures using the thermal EoS combining third-order Birch–Murnaghan EoS and Debye theory along an appropriate geotherm, using the PVT-EoS parameters given in **Table 2**. The resultant density changes of individual phases along the geotherm are depicted in **Figure 9**. The density changes in the bulk rocks were then calculated using the proportions of the individual phases with pressure along the geotherm.

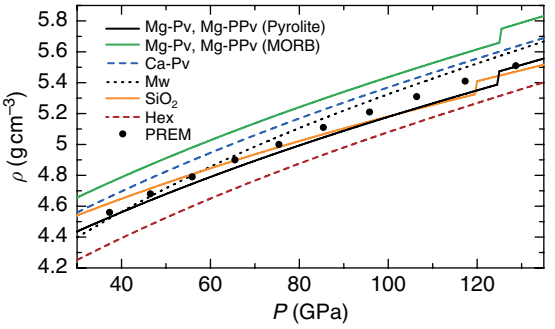

Figure 9 Density changes in major minerals constituting pyrolite and MORB compositions as a function of pressure along the adiabatic geotherm, calculated with EoS using the mineral physics parameters listed in **Table 2**. The density changes of Mg-Pv and Mw in the harzburgite composition are very close to but slightly lower than those of the corresponding phases in pyrolite, which are not shown in this figure. Dots represent the densities in PREM. Hex, hexagonal aluminous phase.

Although some recent studies suggested that sub-adiabatic temperature gradients are required to match the observed and calculated density and bulk sound velocity for pyrolitic compositions (Bina, 2003; Mattern *et al.*, 2005), we simply assumed adiabatic temperature changes throughout the lower mantle (i.e., 1900 K at 660 km and 2450 K at 2890 km with an averaged gradient of $dT/dz = \sim 0.3\,K\,km^{-1}$; e.g., Brown and Shankland, 1981) as such conclusions are not robust, given the uncertainties in both mineral physics measurements and seismological observations and also due to inaccessibility of shear properties of high-pressure phases. In addition, significantly sharp temperature increases are expected to occur near the mantle–core boundary and presumably near the 660 km discontinuity, as these regions are accompanied by chemical changes and form thermal boundary layers (which are also not taken into account in the present calculations).

The mineral proportion changes in pyrolite, harzburgite, and MORB compositions are shown in **Figure 10**, while the calculated density changes of these lithologies are depicted in **Figure 11**. The density changes at pressures lower than 30 GPa are based on an earlier estimate of Irifune (1993), using the similar method and mineral physics parameters. Although the density change in pyrolite seems to agree well with that of PREM (Dziewonski and Anderson, 1981), the latter estimate inevitably has significant uncertainties, as this density profile is rather indirectly determined from seismic velocities with some assumptions. The calculated density values may also have significant errors mainly due to the uncertainty in the geotherm stated in the above. Nevertheless, mineral physics parameters to constrain the density have been reasonably well determined, mostly on the basis of *in situ* X-ray diffraction measurements, and the differences among these calculated density profiles are regarded as robust results.

2.03.4.2 Phase and Density Relations

2.03.4.2.1 Pyrolite

Figure 10(**a**) illustrates the phase transitions in pyrolite as a function of depth. Pyrolite transforms from an assemblage of ringwoodite (Rw) + majorite garnet (Mj) + Ca-Pv under the P,T conditions of the mantle transition region to that of Mg-Pv + Ca-Pv + Mj + Mw at depths near the 660 km seismic discontinuity. The spinel to post-spinel transition in this composition has actually been believed to occur at pressures near 23.5 GPa, at a temperature of ~2000 K, on the basis of quench experiments (e.g., Irifune, 1994). The slope of this phase transition boundary has also been determined by both quench experiments (Ito and Takahashi, 1989) and calorimetric measurements (Akaogi and Ito, 1993), yielding a value of *c.* $-3\,MPa\,K^{-1}$. Although some recent studies suggested somewhat lower transition pressures and larger Clapeyron slope, the spinel to postspinel transition is generally believed to be the main cause of the 660 km discontinuity, which is followed by the smeared-out transition of majorite to Pv over a pressure interval of ~2 GPa (Irifune, 1994; Nishiyama *et al.*, 2004).

Mg-Pv is stable throughout most regions of the lower mantle, but it is found to transform to the Mg-PPv with the $CaIrO_3$ structure in a peridotite composition at pressures close to those near the top of the D″ layer. A small density jump of about 1–1.5% is expected to occur associated with this transition in the lower mantle. Ca-Pv, on the other hand, is likely to remain in the Pv structure throughout the lower mantle. On the other hand, Mw remains in the rock salt (B1) structure at pressures to ~80 GPa, where it may transform to the NiAs (B8) structure if iron concentration is very high (Fei and Mao, 1994). An HS-to-LS transition has also been suggested to occur in this phase over the pressure range of the entire lower mantle, as shown in **Figure 6**, which may yield an additional gradual density increase over this interval and also affect partitioning of iron between this phase and the ferrosilicate Pv.

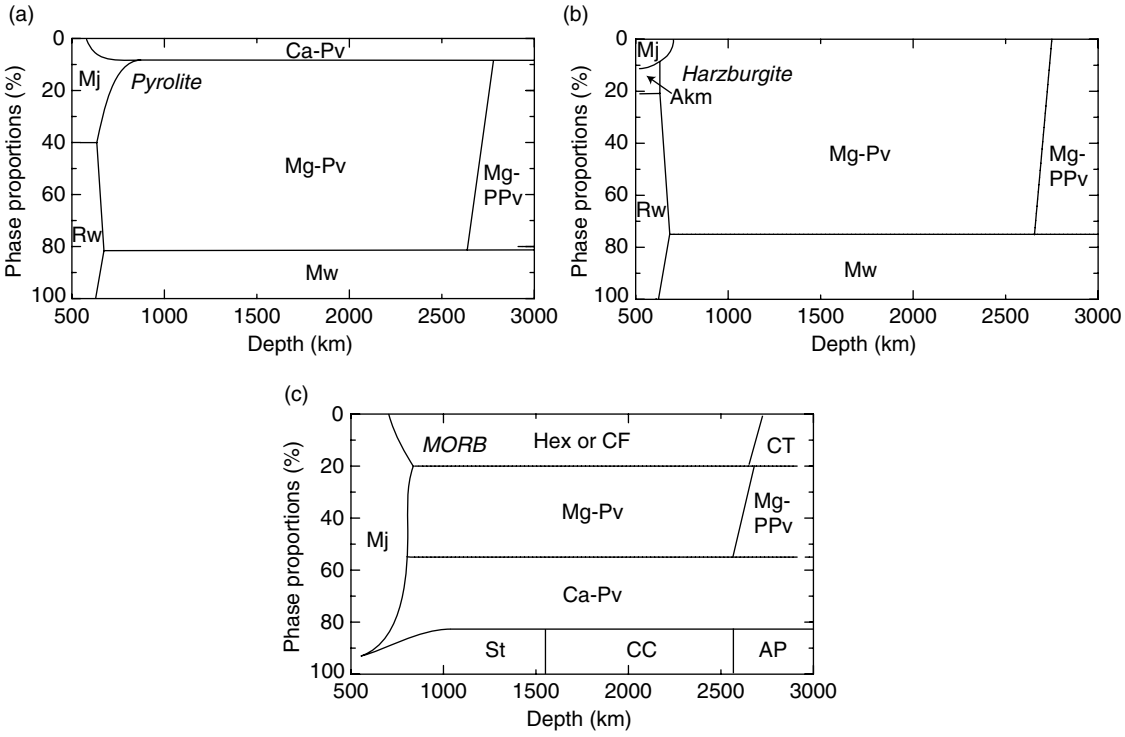

Figure 10 Mineral proportion changes in (a) pyrolite, (b) harzburgite, and (c) MORB as a function of depth along the adiabatic geotherm. Data source: Irifune and Ringwood (1987, 1993); Irifune (1994); Hirose *et al*. (1999, 2005); Murakami *et al*. (2004a, 2005); Ono *et al*. (2001, 2005d). Akm, akimotoite; Rw, ringwoodite; CF, calcium-ferrite phase; CT, calcium-titanite phase; CC, $CaCl_2$ phase; AP, α-PbO_2 phase.

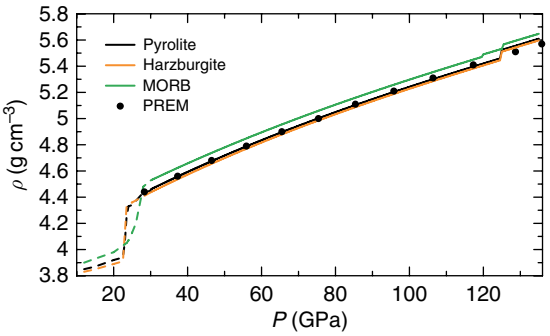

Figure 11 Bulk density variations of pyrolite, hartzburgite, and MORB calculated, based on the PVT-EoS of constituent mineral phases (**Table 1** and **Figure 9**) and their proportions (**Figure 10**). Broken lines at pressures lower than 30 GPa are results in Irifune (1993).

Although element partition data among the coexisting phases under the lower-mantle conditions have been limited to those below ~30 GPa in KMA for the pyrolite composition (e.g., Irifune, 1994; Wood, 2000), some results have also been obtained using LHDAC combined with ATEM at higher pressures (e.g., Murakami *et al*., 2005; Ono *et al*., 2005d). These studies demonstrated that the presence of a minor amount (~5 wt.%) of Al_2O_3 in Mg-Pv has dramatic effects on the partitioning of iron between Mg-Pv and Mw, in addition to those on the compressibility of Mg-Pv. Nevertheless, the variations in iron partitioning between the two phases would not cause any significant changes in the bulk density of the pyrolitic mantle (e.g., Bina, 2003). Some changes in the iron partitioning between Mg-Pv and Mw have also been suggested upon the Pv–PPv transition in a recent LHDAC study (Murakami *et al*., 2005), but it may also yield invisible effects on the density change in the pyrolite bulk composition.

2.03.4.2.2 Harzburgite

Harzburgite, with Mg# (= Mg/(Mg + Fe) × 100) = ~ 92 as listed in **Table 1**, crystallizes to form an assemblage of ~80% olivine and ~20% orthopyroxene at depths of the uppermost mantle, which transforms to Mg-Pv and Mw near the 660 km discontinuity via an assemblage of Rw + Mj + akimotite (Akm, ilmenite form of $MgSiO_3$) as shown by Irifune

and Ringwood (1987). Although no experimental data have been available at pressures higher than 26 GPa, the nature of the phase transition in this composition can be evaluated based on the changes in these two phases under the lower-mantle conditions. The result estimated along the adiabatic geotherm is shown in **Figure 10**(**b**), which shows that this lithology is less dense than pyrolite throughout the lower mantle except for a very limited region immediately below the 660 km discontinuity (Irifune and Ringwood, 1987), where the density relation reverses due to the completion of the spinel to post-spinel transition at lower pressures in the harzburgite composition.

It is likely that Fe significantly lowers the Pv–PPv transition pressure (Mao *et al.*, 2004, 2005), while the presence of Al seems to increase this transition pressure (Tsuchiya *et al.*, 2005c; Tateno *et al.*, 2005), as shown in **Figures 2–4**. In harzburgite compositions, Mg-Pv should have less alumina and iron contents as compared with those of Mg-Pv in pyrolite under the lower-mantle conditions. Thus the pressures of the Pv–PPv transitions in these two compositions may be close to each other due to the opposite effects of Fe and Al, although further detailed experimental studies on these compositions are needed to resolve this issue.

2.03.4.2.3 MORB

Phase transitions in basaltic compositions, such as illustrated in **Figure 10**(**c**) for a MORB composition, are quite different from those expected in pyrolite and harzburgite compositions. Basaltic compositions are shown to crystallize to Mj + small amounts of stishovite (St) in the mantle transition region (Irifune and Ringwood, 1987, 1993; Hirose *et al.*, 1999; Ono *et al.*, 2001), which progressively transform to an assemblage of Ca-Pv + Mg-Pv + St + Al-rich phase (hexagonal or CF/CT structures) over a wide pressure range of ~3 GPa (from ~24 to ~27 GPa). Although the garnetite facies of MORB, composed mainly of Mj, is substantially denser than pyrolite, a density crossover is expected to occur in a limited depth range (660 to ~720 km) of the uppermost lower mantle due to this smeared-out nature of the garnetite-to-Pv transition in MORB.

Once Ca-Pv and Mg-Pv are formed in basaltic compositions, it is shown that they become denser than pyrolite or peridotite throughout almost the entire region of the lower mantle (Irifune and Ringwood, 1993; Hirose *et al.*, 1999, 2005; Ono *et al.*, 2001, 2005d). As St is highly incompressible (**Figure 9**), the density of the perovskite facies of basaltic compositions may approach that of the pyrolitic composition with increasing pressure. However, the transition of St to $CaCl_2$ (CC) and α-PbO_2 (AP) structures should keep this lithology denser than pyrolite throughout the lower mantle, as shown in **Figure 11**. In fact, most recent experimental studies using LHDAC (Ono *et al.*, 2005d; Hirose *et al.*, 2005) conclude that densities of basaltic compositions are higher than those in the representative model mantle compositions throughout the lower mantle by about 0.02–0.08 g cm^{-3}, depending on the adopted pressure scale for gold.

2.03.5 Mineralogy of the Lower Mantle

2.03.5.1 The 660 km Discontinuity

The 660 km seismic discontinuity is a globally recognized feature, and is the sharpest among the proposed discontinuities throughout the whole mantle. The cause of this discontinuity, chemical or phase transition boundary, has been a major controversial issue in Earth sciences as stated earlier, but the detailed experimental study based on quench experiments using KMA strongly suggested that this is caused by the spinel to post-spinel transition in a pyrolite or peridotitic mantle (Ito and Takahashi, 1989; Irifune, 1994). The experimental data on the sharpness, pressure, and Clapeyron slope of this phase transition all seemed to be consistent with those estimated from seismological observations.

However, some recent experimental, seismological, and geodynamics studies cast some doubt on the simple idea of the phase transition. Precise *in situ* X-ray diffraction measurements using KMA demonstrated that this transition occurs at pressures somewhat (~2.5–1 GPa) lower than that correspond to the 660 km discontinuity (Irifune *et al.*, 1998a; Matsui and Nishiyama, 2002; Nishiyama *et al.*, 2004; Fei *et al.*, 2004; Katsura *et al.*, 2003), although some LHDAC experiments reported that the phase transition pressure is consistent with that of the discontinuity (Shim *et al.*, 2001a; Chudinovskikh and Boehler, 2001). Seismological observations also suggest this discontinuity is divided into several discontinuities in some areas (Simmons and Gurrola, 2000), which cannot be explained by the spinel to post-spinel transition alone.

Moreover, recent *in situ* X-ray diffraction measurements have suggested that the Clapeyron slope of the spinel to post-spinel transition is significantly

larger (-2 to $-0.4\,\mathrm{MPa\,K^{-1}}$; Katsura *et al.*, 2003; Fei *et al.*, 2004; Litasov *et al.*, 2005) than previously thought (*c.* $-3\,\mathrm{MPa\,K^{-1}}$; Ito and Takahashi, 1989; Akaogi and Ito, 1993) and *ab initio* prediction (*c.* $-2\,\mathrm{MPa\,K^{-1}}$; Yu *et al.*, 2006). If this is the case, it should be difficult to trap the subducted slabs underneath many subduction zones near this boundary, known as 'stagnant slabs', (e.g., Fukao *et al.*, 1992, 2001; Zhao, 2004), in the light of geodynamics calculations (e.g., Davis, 1998). Moreover, the observed depth variations of the 660 km discontinuity sometimes reach ~30–40 km (e.g., Flanagan and Shearer, 1998), which corresponds to a temperature difference of ~1000 K if we adopt $\mathrm{d}P/\mathrm{d}T = -1\,\mathrm{MPa\,K^{-1}}$ for the spinel–post-spinel transition boundary. Such a temperature difference between subducting slabs and the surrounding mantle near the 660 km discontinuity should be too large to be accounted for by seismological tomographic observations and also by any reasonable models of thermal structures of the subducting slabs.

Nevertheless, considering the uncertainties in pressure and temperature measurements in the *in situ* X-ray observations in KMA due to unresolved problems on the pressure scales and temperature measurements at high pressure using thermocouple emf, it is generally accepted that the 660 km discontinuity can be explained by the spinel–post-spinel transition in a pyrolitic mantle. Recent studies also suggested possibilities of elucidating the multiple nature and the depth variation of the 660 km discontinuity by reactions involving akimotite at relatively low temperatures (Weidner and Wang, 2000; Hirose, 2002). In this case, the high velocity/density gradients shown in some representative seismological models at depths of 660–750 km may be largely explained by the smeared-out transition of majorite to perovskite in pyrolite over this depth interval (Irifune, 1994).

Models with chemical composition changes may reconcile the contradictory experimental and seismological observations regarding the 660 km discontinuity. If the spinel–post-spinel transition does occur at pressures lower than that of 660 km (~23.5 GPa) by, for instance, 1 GPa, the phase discontinuity should locate at about 630 km in a pyrolite mantle. As the oceanic crust component of the subducted slab, modeled by the MORB composition, becomes less dense than the surrounding pyrolite mantle immediately below this depth as shown in **Figure 11**, it should have been buoyantly trapped on this primordial '630 km discontinuity' at the initial stage of the onset of operation of plate tectonics.

The delamination and accumulation of the former oceanic crust, transformed to garnetite in the mantle transition region, can be enhanced by its plausible different viscosity relative to the surrounding mantle (Karato, 1997) and extremely slow reaction kinetics upon transition to the denser phase assemblage including Mg-Pv (Kubo *et al.*, 2002). Continuation of this process of trapping basaltic crust over a couple of billion years should yield a thick (on average ~50–100 km, depending on the production rates of oceanic crust and efficiency of the trapping) layer of garnetite near the 630 km discontinuity. The garnetite layer develops both upward and downward from this primordial discontinuity if it isostatically floats on this boundary. The bottom of this garnetite layer eventually reaches 660 km, under which the harzburgite portion of the subducted slab should be present. In fact, a recent mineral physics study suggests the uppermost lower mantle can be Mg rich as compared with the deeper regions (Bina, 2003).

Accumulation of oceanic crust above the 660 km seismic discontinuity was originally proposed by Anderson (1979) to form an eclogite layer in the lower half of the upper mantle and throughout the mantle transition region, who later confined it to the latter region and favored more mafic lithology named 'piclogite' (e.g., Anderson and Bass, 1986; Duffy and Anderson, 1989). Ringwood (1994) also proposed the presence of a thin (*c.* <50 km) layer of former basaltic crust immediately above the lower mantle, as a result of accumulation of relatively young and warm slab materials at the 660 km discontinuity. The above model of thicker garnetite layer is thus in between those proposed by these authors. Precise measurements of elastic-wave velocities on these lithologies under the P,T conditions of the mantle transition region are needed to further test these hypotheses.

2.03.5.2 Middle Parts of the Lower Mantle

The uppermost part of the lower mantle is believed to be structurally and chemically heterogeneous due to the presence of stagnant slabs (Fukao *et al.*, 1992, 2001; Zhao, 2004) which were originally proposed as 'megaliths' on the basis of high-pressure experimental studies (Ringwood and Irifune, 1988; Ringwood, 1994). Moreover, there are some areas where slabs seem to penetrate deep into the lower mantle by tomographic images (e.g., van der Hilst *et al.*, 1997; Fukao *et al.*, 2001), which should contribute to the observed reflection,

refraction, or conversion of seismic waves at these depths. Thus, the presence of subducted slabs in the uppermost lower mantle may at least partly contribute to the transitional nature of the seismic velocities for a depth interval between 660 and ~750 km in some global models of the velocity profiles.

In the deeper parts of the lower mantle, discontinuous changes in seismic velocities have also been suggested to occur, particularly at depths 900–1200 km beneath some subduction areas (Kawakatsu and Niu, 1994; Niu and Kawakatsu, 1996; Kruger *et al.*, 2001; Kaneshima, 2003). As there are no major phase transitions in the mantle material modeled by pyrolite as shown in **Figure 10**(**a**), such discontinuous changes are most likely to be related to the subducted slab materials. Both basaltic and underlain harzburgite layers of such slabs should yield locally high acoustic impedance to produce seismic discontinuities, because these basaltic and harzburgite materials seem to have seismic velocities higher than those of the mantle material (e.g., Bina, 2003), in addition to their lower temperatures compared to the surrounding mantle.

In further deeper parts of the lower mantle (~1200–1850 km in depth), the presence of seismic scattering bodies with a low-velocity signature was recognized (Kaneshima and Helffrich, 1999, 2003; Vinnik *et al.*, 2001). As shown earlier, the most notable phase transition in major minerals in subducted slab and the surrounding mantle materials is the rutile to $CaCl_2$ transition of SiO_2 in subducted former oceanic crust under the P,T conditions of the middle part (~1600 km, corresponding to pressures of ~70 GPa; Tsuchiya *et al.*, 2004c) of the lower mantle. A significant shear softening is expected to occur in stishovite associated with this phase transition (Karki *et al.*, 1997b; Andrault *et al.*, 1998; Shieh *et al.*, 2002). Thus, this transition in subducted basaltic material may explain the signatures of the scatterers observed in the middle part of the lower mantle.

In contrast, tomographic imaging and other seismological studies demonstrate that only little anomalous changes in seismic velocities exist in the middle to lower part of the lower mantle except for regions related to subducted slabs and rising plumes (e.g., Grand *et al.*, 1997; Zhao, 2004; Mattern *et al.*, 2005). As shown in the previous section, no major phase changes have been reported in Mg-Pv, Ca-Pv, and Mw at pressures up to ~120 GPa, except for the slight distortion of cubic Ca-Pv to a tetragonal structure and the possible HS-to-LS transition and the dissociation of Mw. It is expected that the transition in Ca-Pv may not occur at temperatures of the lower mantle, while the spin transition in Mw should occur continuously over a wide pressure range as shown in **Figure 7** and **Figure 6**, respectively. Accordingly, both of these transitions would not cause any notable seismic velocity changes in this region, although further study is required to address the effects of the possible dissociation of Mw. Thus, the relatively homogeneous nature in seismic velocity distributions in the middle to lower part of the lower mantle is consistent with the absence of major phase transitions in the mantle material.

On the other hand, seismological, geochemical, and geodynamical studies suggest that there should be a chemically distinct region at depths below 1500–2000 km, presumably due to iron enrichment related to the primitive mantle materials or interaction with the rising hot plumes (e.g., Kellogg *et al.*, 1999; Ishii and Tromp, 1999; Trampert *et al.*, 2004). Attempts have been made to estimate the chemical composition of the lower mantle by mineral physics tests (e.g., Jackson and Rigden, 1998; Bina, 2003; Mattern *et al.*, 2005), comparing calculated densities and bulk sound velocities of various compositions with those obtained seismologically. However, it is difficult to constrain the chemical composition of the lower mantle without reasonable estimations of thermal structures in this region and of shear properties of the relevant high-pressure phases. Actually, a wide range of chemical compositions from peridotite to chondrities can be accommodated for the acceptable geotherms, although anomalously high X_{Mg} ($=Mg/(Mg+Fe)$) and low X_{Pv} ($=Si/(Mg+Fe)$) and low X_{Mg} and high X_{Pv} are suggested in the uppermost and lowermost ~200 km of the lower mantle, respectively (Bina, 2003).

The possible iron and silica rich nature in the bottom part of the lower mantle may reflect the heterogeneous chemical composition and mineralogy of this region. These silicon-rich signatures can be explained by the presence of subducted oceanic crust materials in this layer, which is denser than the surrounding pyrolitic or harzburgitic lower-mantle materials, as shown in **Figure 11**. Actually, the $CaCl_2$–α-PbO_2 transition in SiO_2 is calculated to take place at 120–125 GPa and 2000–2500 K (Tsuchiya *et al.*, 2004c), which should stabilize the SiO_2-bearing basaltic material in the D″ layer. Moreover, SiO_2 is also expected to exist in this region as a product of the reaction between the solid silicate Pv (or PPv) of the mantle and the molten Fe of the outer core (Knittle and Jeanloz, 1991).

In contrast, the Mg-rich and Si-poor refractory nature of the uppermost part of the lower mantle suggested by Bina (2003) could be due to the presence of accumulated harzburgite-rich bodies of the stagnant slabs. This is mainly because harzburgite is less dense than pyrolite throughout the lower mantle, as is seen in **Figure 11**. Nevertheless, the density difference is not so large, and the thermal anomalies due to subduction of slabs or rising plumes may be more effective in circulation of the harzburgitic materials within the lower mantle.

2.03.5.3 Postperovskite Transition and the D″ Layer

The bottom ~200 km of the lower mantle is known as a highly heterogeneous region on the basis of seismological observations, named as the D″ layer to distinguish it from grossly homogeneous part of the lower mantle above (region D; Bullen, 1949). The horizontally and vertically heterogeneous nature of the D″ layer is primarily because this region is the chemical boundary layer between convective rocky mantle and molten iron core, which inevitably produces a large thermal boundary layer ($\Delta T > \sim 1000$ K; e.g., Williams, 1998) and accordingly yields active reactions of mantle and core materials (e.g., Knittle and Jeanloz, 1991), partial melting of mantle and slab materials (Lay *et al.*, 2004), generation of hot mantle plumes (Garnero *et al.*, 1998), etc. Various models have been proposed to account for the observed complex seismological signatures of D″ as reviewed by Garnero *et al.* (2004).

The recent finding of the Pv–PPv transition in $MgSiO_3$ has dramatically affected the conventional interpretations of the complex and heterogeneous features of the D″ layer. Many researchers in different research fields of Earth sciences, including mineral physics, seismology, geochemistry, mantle dynamics, etc., have started studies relevant to these topics, and a number of papers have been published immediately after the appearance of the first report on this issue (Murakami *et al.*, 2004a). As the rates of accumulating data are so fast and the relevant research fields so vast, we are unable to thoroughly evaluate all of these studies at this moment. So, instead of discussing the origin of the D″ layer based on rather immature knowledge in these broad research fields, we herein summarize and examine currently available phase relations and some physical properties of the PPv in terms of high-pressure experimental and theoretical points of view. We will make some discussion and speculations on the nature of the D″ layer within these mineral physics frameworks.

Now, what is most robust is that the Pv–PPv transition in $MgSiO_3$ does occur at pressures near the D″ layer on the basis of both high-pressure experiments and *ab initio* calculations. Also true is that the latter phase adopts the crystal structure of $CaIrO_3$ type, as evident from all of these studies. The density increase in Mg-Pv associated with this transition is most likely to be only 1.2–1.5% as constrained experimentally and predicted by *ab initio* calculations. The remarkable agreements among these independent studies on both experimental and theoretical bases strongly suggest that these should be regarded as facts beyond any doubts.

On the other hand, there are some uncertainties in the phase transition pressure and its temperature dependency. The pressures calculated with different scales in DAC experiments, even for those based on the EoS of gold, may differ by as much as 10–15 GPa at pressures of D″ layer (~120–136 GPa) due to the inaccuracy of the EoS's of pressure reference materials as discussed earlier (see **Figure 1**), and accordingly this transition could be realized only at pressures of the outer core (Shim *et al.*, 2004). Moreover, uncertainties in temperature measurements in LHDAC at these very high pressure regions are fairly large, and are generally ±10–20% of the nominal values. These yield additional uncertainties of greater than 2–5 GPa in pressure measurements in LHDAC. Thus the errors of the transition pressure can be *c.* ±20 GPa for the Pv–PPv transition in $MgSiO_3$ within the current state-of-the-art LHDAC technology. Moreover, it is fair to say the Clapeyron slope of this transition has been virtually unconstrained by LHDAC experiments.

In contrast, remarkably good agreement in phase transition pressures (~110 GPa, at 0 K) and the Clapeyron slopes (7–10 MPa K^{-1}) have been obtained in some independent *ab initio* calculations (Tsuchiya *et al.*, 2004a; Oganov and Ono, 2004), which are consistent with the experimental results and also with what are expected by seismological observations (Sidorin *et al.*, 1999). The mutual agreement among the results of the *ab initio* calculations, however, does not warrant the validity of these values, as these authors used basically the same technique with only some relatively minor difference in computational methods and techniques. Thus these results on the Pv–PPv phase boundary based on *ab initio* calculations should be further tested on the basis of experimental studies, before they are regarded as robust ones.

Nevertheless, there is no strong evidence against the occurrence of the Pv–PPv transition at pressures

about 120 GPa, with a Clapeyron slope of 7–10 MPa K^{-1}, and it is reasonable to tentatively take these values as realistic ones. It has been reported that such a large Clapeyron slope is expected to affect the thermal structure of the lower mantle and thus enhances the mantle convection and plume dynamics (Nakagawa and Tackley, 2004). For actual mantle compositions, effects of relatively minor elements such as Fe and Al should be taken into account, but, as we mentioned earlier, these may have opposite effects in modifying the transition pressure, which should be cancelling out each other. Actually, recent experimental results demonstrated that the Pv–PPv transition in peridotitic compositions occurs at pressures close to 120 GPa (Murakami *et al.*, 2005; Ono *et al.*, 2005d). Although a smeared-out transition is expected for this transition when some iron is incorporated in $MgSiO_3$ (Mao *et al.*, 2004, 2005), these studies on the rock samples indicate that the pressure interval of the mixed phase region of Pv and PPv is not so large, suggesting the occurrence of a sharp boundary (Wysession *et al.*, 1998). It is also demonstrated that the PPv phase in the peridotite composition is highly magnesium rich relative to Mw (Murakami *et al.*, 2005), whereas PPv is reported to favor iron compared with Pv in other experimental studies (Mao *et al.*, 2004, 2005; cf. Kobayashi *et al.*, 2005).

Another striking feature of PPv is its elasticity, as predicted by *ab initio* calculations (Tsuchiya *et al.*, 2004b; Oganov and Ono, 2004; Iitaka *et al.*, 2004). The predicted seismic wave speeds of PPv are slightly faster in V_P and V_S and slower in V_Φ than those of Pv at the transition P,T condition as typically observed at the D″ discontinuities (Lay *et al.*, 2004). These velocity changes across the transition boundary seem to explain the enigmatic anticorrelated anomaly between V_S and V_Φ observed at the bottom of the mantle (Wookey *et al.*, 2005; Wentzcovitch *et al.*, 2006). Also, they can vary with changing the iron and aluminum contents in Pv and PPv (Tsuchiya and Tsuchiya, 2006).

Because of the peculiar crystal structure of PPv, which is highly compressible along the *b*-direction, this phase is suggested to be elastically quite anisotropic. The *ab initio* studies also reported that PPv polycrystalline aggregates with lattice-preferred orientation around some crystallographic directions produced by macroscopic stress appear to explain the observed anisotropic propagation of seismic waves in some regions of the D″ layer. In particular, some *ab initio* studies on high-temperature elasticity (Stackhouse *et al.*, 2005a; Wentzcovitch *et al.*, 2006) showed that the transversely isotropic aggregates of PPv can yield horizontally polarized S wave (SH) which travels faster than vertically poralized S wave (SV) at the lower-mantle P,T conditions, as observed underneath Alaska and Central America (Lay *et al.*, 2004). However, the peculiar nature of its shear elasticity suggests that the simple shear motion along the layered structure may not be applicable to the PPv phase at relevant pressures (Tsuchiya *et al.*, 2004b). Moreover, it was predicted that Mw would have substantially large elastic anisotropy under the lower-mantle conditions (Yamazaki and Karato, 2002), suggesting that the PPv phase may not be important in producing anisotropic nature in the D″ layer.

The most likely region, where the Pv–PPv transition plays important roles in the D″ layer, is probably underneath some of the subduction zones, where the temperatures are expected to be relatively lower than that of the surrounding mantle. In these relatively cold regions in the D″ layer, it is known that a sharp discontinuity exists on the top of this layer, under which the highly anisotropic nature of propagation of SV and SH has also been recognized. If this discontinuity corresponds to the Pv–PPv transition, then one of the most likely features of this transition, that is, its large Clapeyron slope of $dP/dT = 7$–10 MPa K^{-1}, suggests that such discontinuity may not exist in warmer regions. For instance, if the temperature in the warmer region is higher than the cold areas by several hundred degrees (such a lateral temperature variation is very likely to exist in the CMB region), this transition would occur in the middle of the D″ layer. However, as the temperature is expected to increase sharply toward the CMB within the D″ layer, the geotherm in the warmer region may not cross the Pv–PPv phase boundary as illustrated in **Figure 12**. In contrast, it is interesting to see that there is a possibility that the geotherm in the colder region might cross the boundary twice, as suggested by recent computational modeling (Hernlund *et al.*, 2005; Wookey *et al.*, 2005).

Thus, if the transition pressure and the Clapeyron slope of the Pv–PPv transition predicted by *ab initio* calculations are correct, many of the observed features in the CMB region can be explained. In warmer regions such as underneath Hawaii or South Africa, this transition would not have any significant roles in producing the peculiar features, such as the presence of ultra-low-velocity region or a large low-velocity structure in these regions, which should be attributed to other phenomena, such as partial melting of the D″ layer material or chemical changes (e.g., Lay *et al.*,

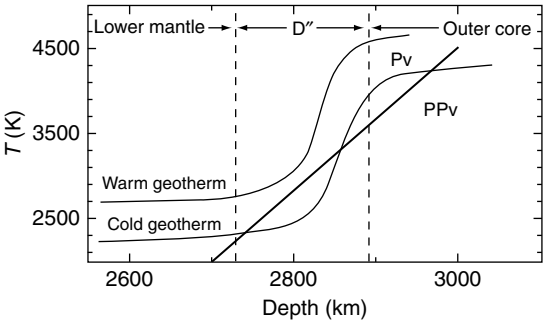

Figure 12 A schematic illustration of the plausible thermal structure at the bottom of the lower mantle, where a steep temperature gradient should be realized due to the formation of the thermal boundary layer. Only the subadiabatic cold geotherm may cross the Pv–PPv phase boundary, and the PPv phase may be sandwiched by Pv because of the shallow slope of this transition and the sharp temperature increase in this region (Hernlund *et al.*, 2005).

2004). Reactions between Mg-Pv in the warm regions with liquid iron may produce an iron-rich PPv phase in these regions, which could also contribute to the observed low velocities in these regions, as suggested by Mao *et al.* (2005). Such reactions between Pv (or PPv) and molten iron should be further explored experimentally to address the nature of the (ultra-)low-velocity zones within the D″ layer.

2.03.6 Summary

Recent advances in both experimental and computational techniques have enabled the quantitative study of phase transitions and mineral physics properties under the lower-mantle P,T conditions. Although uncertainties in pressure and temperature are of the order of ~10% of the nominal values in typical experiments of LHDAC, this apparatus can now produce pressures and temperatures equivalent to those of the entire mantle of the Earth. In contrast, pressures available in KMA have long been limited to ~30 GPa in spite of its superiority in the accuracy of $P-T$ measurements over LHDAC. However, recent developments in KMA using SD anvils doubled this pressure limit, allowing detailed mineral physics studies down to the middle part of the lower mantle.

The accuracy of the mineral physics studies based on *ab initio* calculations has also been dramatically improved in the last decade. A variety of methods and techniques have been developed for the practical applications of DFT to mineral physics studies at very high pressure and temperature. As a result, remarkable agreements among the results from different research groups have been obtained for the phase transition pressures, elastic properties, etc., of some high-pressure phases under the lower-mantle pressures. Thus, such mineral physics properties of high-pressure phases in the lower mantle can now be evaluated and cross-checked on the basis of *ab initio* calculations and the independent experimental studies using LHDAC and KMA.

Phase transitions in major and minor minerals relevant to the mantle and subducted slabs have been studied by using the above independent methods, which clarified structural phase transitions in most of these minerals at pressures and temperatures characteristic of the lower mantle, although there remain some controversial results on the phase transition pressures, their temperature dependencies, element partitioning among the coexisting phases, etc. Although the elastic properties of high-pressure phases, particularly shear properties, have not well documented under the lower-mantle conditions, EoS parameters of some of these phases have successfully been determined by a combination of synchrotron source and KMA-LHDAC or by *ab initio* methods. Thus the density changes in representative mantle and slab compositions can be reasonably evaluated on the basis of the thermoelastic data on individual high-pressure phases and mineral proportion changes in these compositions.

The 660 km discontinuity has conventionally been interpreted in terms of the spinel–post-spinel phase transition in Mg_2SiO_4. However, results of the recent experimental, seismological, and geodynamics studies do not seem to be totally consistent with this interpretation. The presence of a basaltic garnetite layer, as a result of accumulation of subducted oceanic crust materials, may explain such inconsistency and the complex structure near the 660 km discontinuity. The validity of this and other classes of mineralogical models relevant to the origin of the 660 km discontinuity can be evaluated on the basis of mineral physics tests, when accurate elastic-wave velocity data become available for the pyrolite and basaltic compositions under the P,T conditions corresponding to these depths.

The middle part of the lower mantle is believed to be generally homogeneous in both mineralogy and chemistry, as compared with those in the uppermost and lowermost parts of the lower mantle. No major phase transitions are expected to occur in the subducted slab lithologies and the surrounding mantle under the P,T conditions of this part of the lower

mantle, except for the rutile-to-$CaCl_2$ transition in SiO_2 and HS-to-LS transition in Mw (and perhaps Pv). The seismic scatterers of presumably flat bodies found in the middle part of the lower mantle should be related to this phase transition in the former subducted oceanic crust, which may subduct into the deep lower mantle once it passes the density crossover near the 660 km discontinuity. Thus, some parts of the basaltic component of the slab may ultimately reach the bottom of the lower mantle because of its higher density relative to the mantle materials throughout the lower mantle. In contrast, harzburgite-rich layer may be present in the upper part of the lower mantle as a result of accumulation of main bodies of stagnant slabs in this region. However, as the density difference between this layer and the surrounding mantle is not large, thermal effects should be predominant over the chemical effects in gravitational stability of such a layer in the upper part of the lower mantle.

The recently discovered Pv–PPv transition should have significant implications for the structure, properties, and dynamics of the D″ layer, although its actual presence in this region has not been fully proved. Nevertheless, some properties, such as Clapeyron slope, transition pressure, elastically anisotropic nature, and density increase, relevant to the PPv transition seem to be consistent with the seismologically observed signatures in some places of the D″ layer. Further detailed and more accurate experimental studies on this transition are required based on independent techniques using KMA, or LHDAC with improved accuracy, in addition to the theoretical studies and establishment of reliable pressure scales, to understand the nature of this region of the lower mantle.

References

Akahama Y, Kawamura H, and Singh AK (2002) The equation of state of Bi and cross-checking of Au and Pt scales to megabar pressure. *Journal of Physics, Condensed Matter* 14: 11495–11500.

Akahama Y, Kawamura H, and Singh AK (2004) A comparison of volume compressions of silver and gold to 150 GPa. *Journal of Applied Physiology* 95: 4767–4771.

Akaogi M and Ito E (1993) Refinement of enthalpy measurement of $MgSiO_3$ perovskite and negative pressure-temperature slopes for perovskite-forming reactions. *Geophysical Research Letters* 20: 1839–1842.

Akaogi M, Hamada Y, Suzuki T, Kobayashi M, and Okada M (1999) High pressure transitions in the system $MgAl_2O_4$–$CaAl_2O_4$: A new hexagonal aluminous phase with implication for the lower mantle. *Physics of Earth and Planetary Interiors* 115: 67–77.

Akber-Knutson S, Steinle-Neumann G, and Asimow PD (2005) Effect of Al on the sharpness of the $MgSiO_3$ perovskite to post-perovskite phase transition. *Geophysical Research Letters* 32: L14303 (doi:10.1029/2005GL023192).

Alfé D, Alfredsson M, Brodholt J, Gillan MJ, Towler MD, and Needs RJ (2005) Quantum Monte Carlo calculations of the structural properties and the B1–B2 phase transition of MgO. *Physical Review B* 72: 014114.

Anisimov VI, Zaanen J, and Andersen OK (1991) Band theory and Mott insulators: Hubbard U instead of Stoner I. *Physical Review B* 44: 943–954.

Anderson DL (1979) The upper mantle: Eclogite? *Geophysical Research Letters* 6: 433–436.

Anderson DL and Bass JD (1986) Transition region of the Earth's upper mantle. *Nature* 320: 321–328.

Anderson DL (1989) Composition of the Earth. *Science* 243: 367–370.

Anderson OL, Isaak DG, and Yamamoto S (1989) Anharmonicity and the equation of state for gold. *Journal of Applied Physiology* 65: 1534–1543.

Andrault D, Fiquet G, Guyot F, and Hanfland M (1998) Pressure-induced Landau-type transition in stishovite. *Science* 282: 720–724.

Andrault D, Angel RJ, Mosenfelder JL, and Bihan TLe (2003) Equation of state of stishovite to lower mantle pressures. *American Mineralogist* 88: 1261–1265.

Badro J, Struzhkin VV, Shu J, *et al.* (1999) Magnetism in FeO at megabar pressures from X-ray emission spectroscopy. *Physical Review Letters* 83: 4101–4104.

Badro J, Fiquet G, Guyot F, *et al.* (2003) Iron partitioning in Earth's mantle: Toward a deep lower mantle discontinuity. *Science* 300: 789–791.

Badro J, Rueff J-P, Vankó G, Monaco G, Fiquet G, and Guyot F (2004) Electronic transitions in perovskite: Possible nonconvecting layers in the lower mantle. *Science* 305: 383–386.

Bagno P, Jepsen O, and Gunnarsson O (1989) Ground-state properties of third-row elements with nonlocal density functionals. *Physical Review B* 40: 1997–2000.

Beck P, Gillet P, Gautron L, Daniel I, and El Goresy A (2004) A new natural high-pressure (Na,Ca)-hexaluminosilicate $[(Ca_xNa_{1-x})Al_{3+x}Si_{3-x}O_{11}]$ in shocked Martian meteorites. *Earth and Planetary Science Letters* 219: 1–12.

Biellmann C, Gillet P, Guyot F, Peyronneau J, and Reyard B (1993) Experimental evidence for carbonate stability in Earth's lower mantle. *Earth and Planetary Science Letters* 118: 31–41.

Bina CR (2003) Seismological constraints upon mantle composition. In: Carlson R (ed.) *Treatise on Geochemistry*, vol. 2, pp. 39–59. Amsterdam: Elsevier.

Birch F (1952) Elasticity and constitution of the Earth's interior. *Journal of Geophysical Research* 57: 227–286.

Brown JM and Shankland TJ (1981) Thermodynamic parameters in the Earth as determined from seismic profiles. *Geophysical Journal of the Royal Astronomical Society* 66: 579–596.

Bullen KE (1949) Compressibility-pressure hypothesis and the Earth's interior. *MNRAS. Geophysical Supplement* 5: 355–368.

Caracas R and Cohen RE (2005a) Prediction of a new phase transition in Al_2O_3 at high pressures. *Geophysical Research Letters* 32: L06303 (doi:10.1029/2004GL022204).

Caracas R and Cohen RE (2005b) Effect of chemistry on the stability and elasticity of the perovskite and post-perovskite phases in the $MgSiO_3$–$FeSiO_3$–Al_2O_3 system and implications for the lowermost mantle. *Geophysical Research Letters* 32: L16310 (doi:10.1029/2005GL023164).

Caracas R, Wentzcovitch R, Price GD, and Brodholt J (2005) $CaSiO_3$ perovskite at lower mantle pressures. *Geophysical Research Letters* 32: L06306 (doi:10.1029/2004GL022144).

Catti M (2001) High-pressure stability, structure and compressibility of *Cmcm*-$MgAl_2O_4$: An *ab initio* study. *Physics and Chemistry of Minerals* 28: 729–736.

Chizmeshya AVG, Wolf GH, and McMillan PF (1996) First principles calculation of the equation-of-state, stability, and polar optic modes of $CaSiO_3$ perovskite. *Geophysical Research Letters* 23: 2725–2728.

Chudinovskikh L and Boehler R (2001) High-pressure polymorphs of olivine and the 660-km seismic discontinuity. *Nature* 411: 574–577.

Cococcioni M and de Gironcoli S (2005) Linear response approach to the calculation of the effective interaction parameters in the LDA+U method. *Physical Review B* 71: 035105.

Cohen RE, Mazin, II, and Isaak DG (1997) Magnetic collapse in transition metal oxides at high pressure: implications for the Earth. *Science* 275: 654–657.

Davis GF (1998) Plates, plumes, mantle convection, and mantle evolution. In: Jackson I (ed.) *The Earth's Mantle*, pp. 228–258. New York: Cambridge University Press.

Demuth Th, Jeanvoine Y, Hafner J, and Ángyán JG (1999) Polymorphism in silica studied in the local density and generalized-gradient approximations. *Journal of Physics, Condensed Matter* 11: 3833–3874.

Dubrovinsky LS, Saxena SK, Lazor P, *et al.* (1997) Experimental and theoretical identification of a new high-pressure phase of silica. *Nature* 388: 362–365.

Dubrovinsky LS, Dubrovinskaia NA, Saxena SK, *et al.* (2000) Stability of Ferropericlase in the lower mantle. *Science* 289: 430–432.

Dubrovinsky LS, Dubrovinskaia NA, Saxena SK, *et al.* (2001) Pressure-induced transformations of cristobalite. *Chemical Physics Letters* 333: 264–270.

Duffy TS and Anderson DL (1989) Seismic velocities in mantle minerals and the mineralogy of the upper mantle. *Journal of Geophysical Research* 94: 1895–1912.

Duffy TS, Hemley RJ, and Mao H-K (1995) Equation of state and shear strength at multimegabar pressures: Magnesium oxide to 227 GPa. *Physical Review Letters* 74: 1371–1374.

Dziewonski AM and Anderson DL (1981) Preliminary reference Earth model. *Physics of Earth and Planetary Interiors* 25: 297–356.

Fei Y and Mao H-K (1994) *In situ* determination of the NiAs phase of FeO at high pressure and high temperature. *Science* 266: 1678–1680.

Fei Y, Van Orman J, Li J, *et al.* (2004) Experimentally determined postspinel transformation boundary in Mg_2SiO_4 using MgO as an internal pressure standard and its geophysical implications. *Journal of Geophysical Research* 109: B02305 1–8.

Ferroir T, Yagi T, Onozawa T, *et al.* (2006) Equation of state and phase transition in $KAlSi_3O_8$ hollandite at high pressure. *American Mineralogist* 91(2–3): 327–332.

Fiquet G, Richet P, and Montagnac G (1999) High-temperature thermal expansion of lime, periclase, corundum and spinel. *Physics and Chemistry of Minerals* 27: 103–111.

Fiquet G, Dewaele A, Andrault D, Kunz M, and Bihan TL (2000) Thermoelastic properties and crystal structure of $MgSiO_3$ perovskite at lower mantle pressure and temperature conditions. *Geophysical Research Letters* 27: 21–24.

Fiquet A, Guyot F, Kunz M, Matas J, Andrault D, and Hanfland M (2002) Structural refinements of magnesite at very high pressure. *American Mineralogist* 87: 1261–1265.

Flanagan MP and Shearer PM (1998) Global mapping of topography on transition zone velocity discontinuities by stacking SS precursors. *Journal of Geophysical Research* 103: 2673–2692.

Frost DJ and Fei Y (1998) Stability of phase D at high pressure and high temperature. *Journal of Geophysical Research* 103: 7463–7474.

Fukao Y, Obayashi M, Inoue H, and Nenbai M (1992) Subducting slabs stagnant in the mantle transition zone. *Journal of Geophysical Research* 97: 4809–4822.

Fukao Y, Widiyantoro S, and Obayashi M (2001) Stagnant slabs in the upper and lower mantle transition region. *Reviews of Geophysics* 39: 291–323.

Funamori N, Yagi T, Utsumi W, Kondo T, and Uchida T (1996) Thermoelastic properties of $MgSiO_3$ perovskite determined by in situ X-ray observations up to 30 GPa and 2000 K. *Journal of Geophysical Research* 101: 8257–8269.

Funamori N and Jeanloz R (1997) High-pressure transformation of Al_2O_3, *Science* 278: 1109–1111.

Funamori N, Jeanloz R, Nguyen JH, *et al.* (1998) High-pressure transformations in $MgAl_2O_4$. *Journal of Geophysical Research* 103: 20813–20818.

Gaffney ES and Anderson DL (1973) Effect of low-spin Fe^{2+} on the composition of the lower mantle. *Journal of Geophysical Research* 78: 7005–7014.

Garnero EJ, Revenaugh JS, Williams Q, Lay T, and Kellogg LH (1998) Ultralow velocity zone at the core-mantle boundary. In: Gurnis M, Wysession M, Knittle E, and Buffett B (eds.) *The Core-Mantle Boundary Region*, pp. 319–334. Washington, DC: AGU.

Garnero EJ, Maupin V, Lay T, and Fouch MJ (2004) Variable azimuthal anisotropy in Earth's lowermost mantle. *Science* 306: 259–261.

Gautron L, Angel RJ, and Miletich R (1999) Structural characterization of the high-pressure phase $CaAl_4Si_2O_{11}$. *Physics and Chemistry of Minerals* 27: 47–51.

Gautron L, Daniel I, Beck P, Gulgnot N, Andrault D, and Greaux S (2005) On the track of 5-fold silicon signature in the high pressure CAS phase $CaAl_4Si_2O_{11}$. *Eos Transactions of the American Geophysical Unioin* 86(52): Fall Meeting Supplement, Abstract MR23C-0087.

Gillet P (1993) Stability of magnesite ($MgCO_3$) at mantle pressure and temperature conditions: A Raman spectroscopic study. *American Mineralogist* 78: 1328–1331.

Gillet P, Chen M, Dubrovinsky LS, and El Goresy A (2000) Natural $NaAlSi_3O_8$-hollandite in the shocked Sixiangkou meteorite. *Science* 287: 1633–1636.

Grand S, van der Hilst R, and Widiyantoro S (1997) Global seismic tomography: a snap shot of convection in the Earth. *GSA Today* 7: 1–7.

Green DH, Hibberson WO, and Jaques AL (1979) Petrogenesis of mid-ocean ridge basalts. In: McElhinny MW (ed.) *The Earth: Its Origin, Structure and Evolution*, pp. 269–299. London: Academic Press.

Hamann DR (1996) Generalized gradient theory for silica phase transitions. *Physical Review Letters* 76: 660–663.

Hamann DR (1997) H_2O hydrogen bonding in density-functional theory. *Physical Review B* 55: R10157–R10160.

Hart SR and Zindler A (1986) In search for a bulk Earth composition. *Chemical Geology* 57: 247–267.

Heinz DL and Jeanloz R (1984) The equation of state of the gold calibration standard. *Journal of Applied Physiology* 55: 885–893.

Helffrich G and Wood B (2001) The Earth's mantle. *Nature* 412: 501–507.

Hernlund JW, Thomas C, and Tackley PJ (2005) A doubling of the post-perovskite phase boundary and structure of the Earth's lowermost mantle. *Nature* 434: 882–886.

Hirose K, Fei Y, Ma Y, and Mao H-K (1999) The fate of subducted basaltic crust in the Earth's lower mantle. *Nature* 397: 53–56.

Hirose K (2002) Phase transition in pyrolitic mantle around 670-km depth: implications for upwelling of plumes from the lower mantle. *Journal of Geophysical Research* 107: 2078 (doi:10.1029/2001JB000597).

Hirose K, Takafuji N, Sata N, and Ohishi Y (2005) Phase transition and density of subducted MORB crust in the lower mantle. *Earth and Planetary Science Letters* 237: 239–251.

Hohenberg P and Kohn W (1964) Inhomogeneous electron gas. *Physical Review* 136: B364–B871.

Holmes NC, Moriarty JA, Gathers GR, and Nellis WJ (1989) The equation of state of platinum to 660 GPa (6.6 Mbar). *Journal of Applied Physiology* 66: 2962–2967.

Iitaka T, Hirose K, Kawamura K, and Murakami M (2004) The elasticity of the $MgSiO_3$ post-perovskite phase in the Earth's lowermost mantle. *Nature* 430: 442–444.

Irifune T and Ringwood AE (1987) Phase transformations in a harzburgite composition to 26 GPa: Implications for dynamical behaviour of the subducting slab. *Earth and Planetary Science Letters* 86: 365–376.

Irifune T, Fujino K, and Ohtani E (1991) A new high-pressure form of $MgAl_2O_4$. *Nature* 349: 409–411.

Irifune T (1993) Phase transformations in the earth's mantle and subducting slabs: Implications for their compositions, seismic velocity and density structures and dynamics. *The Island Arc* 2: 55–71.

Irifune T and Ringwood AE (1993) Phase transformations in subducted oceanic crust and buoyancy relationships at depths of 600–800 km in the mantle. *Earth and Planetary Science Letters* 117: 101–110.

Irifune T (1994) Absence of an aluminous phase in the upper part of the Earth's lower mantle. *Nature* 370: 131–133.

Irifune T, Ringwood AE, and Hibberson WO (1994) Subduction of continental crust and terrigenous and pelagic sediments: An experimental study. *Earth and Planetary Science Letters* 126: 351–368.

Irifune T, Koizumi T, and Ando J (1996a) An experimental study of the garnet-perovskite transformation in the system $MgSiO_3$–$Mg_3Al_2Si_3O_{12}$. *Geophysical Research Letters* 96: 147–157.

Irifune T, Kuroda K, Funamori N, *et al.* (1996b) Amorphization of serpentine at high pressure and high temperature. *Science* 272: 1468–1470.

Irifune T, Nishiyama N, Kuroda K, *et al.* (1998a) The postspinel phase boundary in Mg_2SiO_4 determined by in situ X-ray diffraction. *Science* 279: 1698–1700.

Irifune T, Kubo N, Isshiki M, and Yamasaki Y (1998b) Phase transformations in serpentine and transportation of water into the lower mantle. *Geophysical Research Letters* 25: 203–206.

Irifune T (2002) Application of synchrotron radiation and Kawai-type apparatus to various studies in high-pressure mineral physics. *Mineralogical Magazine* 66: 769–790.

Irifune T, Naka H, Sanehira T, Inoue T, and Funakoshi K (2002) *In situ* X-ray observations of phase transitions in $MgAl_2O_4$ spinel to 40 GPa using multianvil apparatus with sintered diamond anvils. *Physics and Chemistry of Minerals* 29: 645–654.

Irifune T, Isshiki M, and Sakamoto S (2005) Transmission electron microscope observation of the high-pressure form of magnesite retrieved from laser heated diamond anvil cell. *Earth and Planetary Science Letters* 239: 98–105.

Ishii M and Tromp J (1999) Normal-mode and free-air gravity constraints on lateral variations in velocity and density of Earth's mantle. *Science* 285: 1231–1236.

Isshiki M, Irifune T, Hirose K, *et al.* (2004) Stability of magnesite and its high-pressure form in the lowermost mantle. *Nature* 427: 60–63.

Ito E and Takahashi E (1989) Post-spinel transformations in the system. Mg_2SiO_4–Fe_2SiO_4 and some geophysical implications. *Journal of Geophysical Research* 94: 10637–10646.

Ito E, Kubo A, Katsura T, Akaogi M, and Fujita T (1998) High-pressure phase transition of pyrope ($Mg_3Al_2Si_3O_{12}$) in a sintered diamond cubic anvil assembly. *Geophysical Research Letters* 25: 821–824.

Ito E, Katsura T, Aizawa Y, Kawabe K, Yokoshi S, and Kubo A (2005) High-pressure generation in the Kawai-type apparatus equipped with sintered diamond anvils: Application to the wurtzite–rocksalt transformation in GaN. In: Chen J, Wang Y, Duffy TS, Shen G, and Dobrzhinetskaya LF (eds.) *Advances in High-Pressure Technology for Geophysical Applications*, pp. 451–460. Amsterdam: Elsevier.

Jackson I, Khanna SK, Revcolevschi A, and Berthon J (1990) Elasticity, shear-mode softening and high-pressure polymorphism of Wüstite ($Fe_{1-x}O$). *Journal of Geophysical Research* 95: 21671–21685.

Jackson I and Rigden SM (1998) Composition and temperature of the Earth's mantle: Seismological models interpreted through experimental studies of the Earth materials. In: Jackson I (ed.) *The Earth's Mantle*, pp. 405–460. New York: Cambridge University Press.

Jackson JM, Sturhahn W, Shen G, *et al.* (2005) A synchrotron Mössbauer spectroscopy study of $(Mg,Fe)SiO_3$ perovskite up to 120 GPa. *American Mineralogist* 90: 199–205 .

Jacobsen SD, Reichmann HJ, Spetzler HA, *et al.* (2002) Structure and elasticity of single crys tal (Fe,Mg)O and a new method of generating shear waves for gigahertz ultra sonic interferometry. *Journal of Geophysical Research* 107: 1–14 (doi:10.1029 2001JB000490).

Jamieson JC, Fritz JN, and Manghnani MH (1982) Pressure measurement at high temperature in X-ray diffraction studies: Gold as a primary standard. In: Akimoto S, and Manghnani MH (eds.) *High-Pressure Research in Geophysics*, pp. 27–48. Tokyo: Center for Academic Publications.

Jeanloz R and Thompson AB (1983) Phase transitions and mantle discontinuities. *Reviews of Geophysics Space Phys* 21: 51–74.

Kaneshima S and Helffrich G (1999) Dipping low-velocity layer in the mid-lower mantle: Evidence for geochemical heterogeneity. *Science* 283: 1888–1891.

Kaneshima S (2003) Small scale heterogeneity at the top of the lower mantle around the Mariana slab. *Earth and Planetary Science Letters* 209: 85–101.

Kaneshima S and Helffrich G (2003) Subparallel dipping heterogeneities in the mid-lower mantle. *Journal of Geophysical Research* 108: 2272 (doi:10.1029/2001JB001596).

Karato S (1997) On the separation of crustal component from subducted oceanic lithosphere near the 660 km discontinuity. *Physics of Earth and Planetary Interiors* 99: 103–111.

Karki BB, Stixrude L, and Crain J (1997a) *Ab initio* elasticity of three high-pressure polymorphs of silica. *Geophysical Research Letters* 24: 3269–3272.

Karki BB, Warren MC, Stixrude L, Clark SJ, Ackland GJ, and Crain J (1997b) *Ab initio* studies of high-pressure structural transformations in silica. *Physical Review B* 55: 3465–3471.

Karki BB and Crain J (1998) First-principles determination of elastic properties of $CaSiO_3$ perovskite at lower mantle pressures. *Geophysical Research Letters* 25: 2741–2744.

Karaki BB, Wentzcovitch RM, de Gironcoli S, and Baroni S (2000) High-pressure lattice dynamics and thermoelasticity of MgO. *Physical Review B* 61: 8793–8800.

Katsura T and Ito E (1996) Determination of Fe–Mg partitioning between perovskite and magnesiowüstite. *Geophysical Research Letters* 23: 2005–2008.

Katsura T, Yamada H, Shinmei T, *et al.* (2003) Post-spinel transition in Mg_2SiO_4 determined by high P-T *in situ* X-ray diffractometry. *Physics of Earth and Planetary Interiors* 136: 11–24.

Kawai N and Endo S (1970) The generation of ultrahigh hydrostatic pressures by a split sphere apparatus. *Review of Scientific Instruments* 41: 1178–1181.

Kawakatsu H and Niu F (1994) Seismic Evidence for a 920km discontinuity in the mantle. *Nature* 371: 301–305.

Kellogg LH, Hager BH, and van der Hilst RD (1999) Compositional stratification in the deep mantle. *Science* 283: 1881–1884.

Kesson SE, Fitz Gerald JD, and Shelley JM (1998) Mineralogy and dynamics of a pyrolite lower mantle. *Nature* 393: 252–255.

Kiefer B, Stixrude L, and Wentzcovitch RM (2002) Elasticity of $(Mg,Fe)SiO_3$-perovskite at high pressure. *Geophysical Research Letters* 29: 1539 (doi:10.1029/2002GL014683).

Kingma KJ, Cohen RE, Hemley RJ, and Mao HK (1995) Transformation of stishovite to a denser phase at lower-mantle pressures. *Nature* 374: 243–246.

Knittle E and Jeanloz R (1991) Earth's core-mantle boundary: results of experiments at high pressure and temperatures. *Science* 251: 1438–1443.

Kobayashi Y, Kondo T, Ohtani T, *et al.* (2005) Fe-Mg partitioning between $(Mg,Fe)SiO_3$ post-perovskite, perovskite, and magnesiowüstite in the Earth's lower mantle. *Geophysical Research Letters* 32: L19301 (doi:10.1029/2005GL023257).

Kohn W and Sham LJ (1965) Self-consistent equation including exchange and correlation effects. *Physical Review* 140: A1133–A1138.

Kondo T, Ohtani E, Hirao N, Yagi T, and Kikegawa T (2004) Phase transitions of (Mg,Fe)O at megabar pressures. *Physics of Earth and Planetary Interiors* 143-144: 201–213.

Kruger F, Banumann M, Scherbaum F, and Weber M (2001) Mid mantle scatterers near the Mariana slab detected with a double array method. *Geophysical Research Letters* 28: 667–670.

Kubo T, Ohtani E, Kondo T, *et al.* (2002) Metastable garnet in oceanic crust at the top of the lower mantle. *Nature* 420: 803–806.

Kudoh Y, Nagase T, Mizohata H, and Ohtani E (1997) Structure and crystal chemistry of phase G, a new hydrous magnesium silicate synthesized at 22 GPa and 1050°C. *Geophysical Research Letters* 24: 1051–1054.

Kurashina T, Hirose K, Ono S, Sata N, and Ohishi Y (2004) Phase transition in Al-bearing $CaSiO_3$ perovskite: Implications for seismic discontinuities in the lower mantle. *Physics of Earth and Planetary Interiors* 145: 67–74.

Kuroda K and Irifune T (1998) Observation of phase transformations in serpentine at high pressure and high temperature by *in situ* X ray diffraction measurements. In: Manghnani MH and Yagi T (eds.) *High Pressure–Temperature Research: Properties of Earth and Planetary Materials*, pp. 545–554. Washington DC: AGU.

Lay T, Garnero EJ, and Williams Q (2004) Partial melting in a thermo-chemical boundary layer at the base of the mantle. *Physics of Earth and Planetary Interiors* 146: 441–467.

Li J, Struzhkin VV, Mao H-K, *et al.* (2004) Electronic spin state of iron in lower mantle perovskite. *Proceedings of the National Academy of Sciences* 101: 14027–14030.

Li L, Weidner DJ, Brodholt J, *et al.* (2006a) Elasticity of $CaSiO_3$ perovskite at high pressure and high temperature. *Physics of Earth and Planetary Interiors* 155: 249–259.

Li L, Weidner DJ, Brodholt J, *et al.* (2006b) Phase stability of $CaSiO_3$ perovskite at high pressure and temperature: Insights from *ab initio* molecular dynamics. *Physics of Earth and Planetary Interiors* 155: 260–268.

Lin J-F, Heinz DL, Mao H-K, *et al.* (2003) Stability of magnesiowüstite in earth's lower mantle. *Proceedings of the National Academy of Sciences* 100: 4405–4408.

Lin J-F, Struzhkin VV, Jacobsen SD, *et al.* (2005) Spin transition of iron in magnesiowüstite in the Earth's lower mantle. *Nature* 436: 377–380.

Litasov K, Ohtani E, Sano A, Suzuki A, and Funakoshi K (2005) *In situ* X-ray diffraction study of post-spinel transformation in a peridotite mantle: Implication for the 660-km discontinuity. *Earth and Planetary Science Letters* 238: 311–328.

Liu L-G (1977) High pressure $NaAlSiO_4$: The first silicate calcium ferrite isotope. *Geophysical Research Letters* 4: 183–186.

Liu L-G (1978) A new high-pressure phase of spinel. *Earth and Planetary Science Letters* 41: 398–404.

Liu L-G (1982) Speculations on the composition and origin of the Earth. *Geochemical Journal* 16: 287–310.

Liu L-G (1986) Phase transformations in serpentine at high pressures and temperatures and implications for subducting lithosphere. *Physics of Earth and Planetary Interiors* 42: 255–262.

Liu L-G (1999) Genesis of diamonds in the lower mantle. *Contributions to Mineralogy and Petrology* 134: 170–173.

Liu X (2006) Phase relations in the system $KAlSi_3O_8$–$NaAlSi_3O_8$ at high pressure-high temperature conditions and their implication for the petrogenesis of lingunite. *Earth and Planetary Science Letters* 246: 317–325.

Loubet M, Sassi R, and Di Donato G (1988) Mantle heterogeneities: A combined isotope and trace element approach and evidence for recycled continental crust materials in some OIB sources. *Earth and Planetary Science Letters* 89: 299–315.

Magyari-Köpe B, Vitos L, Grimvall G, Johansson B, and Kollár J (2002) Low-temperature crystal structure of $CaSiO_3$ perovskite: An *ab initio* total energy study. *Physical Review B* 65: 193107.

Mao HK, Chen LC, Hemley RJ, Jephcoat AP, and Wu Y (1989) Stability and equation of state of $CaSiO_3$ up to 134 GPa. *Journal of Geophysical Research* 94: 17889–17894.

Mao HK, Hemley RJ, Fei Y, *et al.* (1991) Effect of pressure, temperature and composition on lattice parameters and density of $(Fe,Mg)SiO_3$ -perovskites to 30 GPa. *Journal of Geophysical Research* 96: 8069–8080.

Mao WL, Shen G, Prakapenka VB, *et al.* (2004) Ferromagnesian postperovskite silicates in the D″ layer of the Earth. *Proceedings of the National Academy of Sciences* 101: 15867–15869.

Mao WL, Meng Y, Shen G, *et al.* (2005) Iron-rich silicates in the Earth's D″ layer. *Proceedings of the National Academy of Sciences* 102: 9751–9753.

Marton F and Cohen R (1994) Prediction of a high pressure phase transition in Al_2O_3. *American Mineralogist* 79: 789–792.

Matsui M and Nishiyama N (2002) Comparison between the Au and MgO pressure calibration standards at high temperature. *Geophysical Research Letters* 29: 1368 (doi:10.1029/2001GL014161).

Mattern E, Matas J, Ricard Y, and Bass J (2005) Lower mantle composition and temperature from mineral physics and thermodynamic modeling. *Geophysical Journal International* 160: 973–990.

Mazin II, Fei Y, Downs R, and Cohen R (1998) Possible polytypism in FeO at high pressures. *American Mineralogist* 83: 451–457.

Meade C, Mao HK, and Hu J (1995) High-temperature phase transition and dissociation of $(Mg,Fe)SiO_3$ perovskite at lower mantle pressures. *Science* 268: 1743–1745.

Michael PJ and Bonatti E (1985) Peridotite composition from the North Atlantic: Regional and tectonic variations and implications for partial melting. *Earth and Planetary Science Letters* 73: 91–104.

Miyajima N, Yagi T, Hirose K, Kondo T, Fujino K, and Miura H (2001) Potential host phase of aluminum and potassium in the Earth's lower mantle. *American Mineralogist* 86: 740–746.

Murakami M, Hirose K, Ono S, and Ohishi Y (2003) Stability of $CaCl_2$-type and α-PbO_2-type SiO_2 at high pressure and temperature determined by *in-situ* X-ray measurements. *Geophysical Research Letters* 30: doi:10.1029/2002GL016722.

Murakami M, Hirose K, Kawamura K, Sata N, and Ohishi Y (2004a) Post-perovskite phase transition in $MgSiO_3$. *Science* 304: 855–858.

Murakami M, Hirose K, Ono S, Isshiki M, and Watanuki T (2004b) High pressure and high temperature phase transitions of FeO. *Physics of Earth and Planetary Interiors* 146: 273–282.

Murakami M, Hirose K, Sata N, and Ohishi Y (2005) Post-perovskite phase transition and mineral chemistry in the pyrolitic lowermost mantle. *Geophysical Research Letters* 32: L03304 (doi:10.1029/2004GL021956).

Nakagawa T and Tackley PJ (2004) Effects of a perovskite–post perovskite phase change near core–mantle boundary in compressible mantle convection. *Geophysical Research Letters* 31: L16611 (doi:10.1029/2004GL020648).

Niu F and Kawakatsu H (1996) Complex structure of the mantle discontinuities at the tip of the subducting slab beneath the northeast China: A preliminary investigation of broadband receiver functions. *Journal of the Physics of the Earth* 44: 701–711.

Nishiyama N, Irifune T, Inoue T, Ando J, and Funakoshi K (2004) Precise determination of phase relations in pyrolite across the 660 km seismic discontinuity by in situ X-ray diffraction and quench experiments. *Physics of Earth and Planetary Interiors* 143-144: 185–199.

Nishihara Y (2003) *Density and Elasticity of Subducted Oceanic Crust in the Earth's mantle*, pp.169. Ph.D Thesis, Tokyo Institute of Technology.

Oganov AR, Gillan MJ, and Price GD (2005) Structural stability of silica at high pressures and temperatures. *Physical Review B* 71: 064104.

Oganov AR and Ono S (2004) Theoretical and experimental evidence for a post-perovskite phase of $MgSiO_3$ in Earth's D'' layer. *Nature* 430: 445–448.

Ohtani E, Kagawa N, and Fujino K (1991) Stability of majorite $(Mg,Fe)SiO_3$ at high pressures and 1800°C. *Earth and Planetary Science Letters* 102: 158–166.

Ohtani E, Mizobata H, Kudoh Y, *et al.* (1997) A new hydrous silicate, a water reservoir, in the upper part of the lower mantle. *Geophysical Research Letters* 24: 1047–1050.

Ohtani E, Litasov K, Hosoya T, Kubo T, and Kondo T (2004) Water transport into the deep mantle and formation of a hydrous transition zone. *Physics of Earth and Planetary Interiors* 143–144: 255–269.

Ono S, Ito E, and Katsura T (2001) Mineralogy of subducted basaltic crust (MORB) from 25 to 37 GPa, and chemical heterogeneity of the lower mantle. *Earth and Planetary Science Letters* 190: 57–63.

Ono S, Hirose K, Murakami M, and Isshiki M (2002) Post-stishovite phase boundary in SiO_2 determined by *in situ* X-ray observations. *Earth and Planetary Science Letters* 197: 187–192.

Ono S, Ohishi Y, and Mibe K (2004) Phase transition of Ca-perovskite and stability of Al-bearing Mg-perovskite in the lower mantle. *American Mineralogist* 89: 1480–1485.

Ono S, Kikegawa T, and Ohishi Y (2005a) A high-pressure and high-temperature synthesis of platinum carbide. *Solid State Communications* 133: 55–59.

Ono S, Funakoshi K, Ohishi Y, and Takahashi E (2005b) *In situ* X-ray observation of the phase transition of Fe_2O_3. *Journal of Physics – Condensed Matter* 17: 269–276.

Ono S, Kikegawa T, Ohishi Y, and Tsuchiya J (2005c) Post-aragonite phase transformation in $CaCO_3$ at 40 GPa. *American Mineralogist* 90: 667–671.

Ono S, Ohishi Y, Isshiki M, and Watanuki T (2005d) *In situ* X-ray observations of phase assemblages in peridotite and basalt compositions at lower mantle conditions: Implications for density of subducted oceanic plate. *Journal of Geophysical Research* 110: B02208 (doi:10.1029/2004JB003196).

Parise JB, Wang Y, Yeganeh-Haeri A, Cox DE, and Fei Y (1990) Crystal structure and thermal expansion of $(Mg,Fe)SiO_3$ perovskite. *Geophysical Research Letters* 17: 2089–2092.

Perdew JP, Chevary JA, Vosko SH, *et al.* (1992) Atoms, molecules, solids, and surfaces: Applications of the generalized gradient approximation for exchange and correlation. *Physical Review B* 46: 6671–6687.

Perdew JP, Burke K, and Ernzerhof M (1996) Generalized gradient approximation made simple. *Physical Review Letters* 77: 3865–3868.

Ringwood AE (1962) A model for the upper mantle. *Journal of Geophysical Research* 67: 857–867.

Ringwood AE and Irifune T (1988) Nature of the 650-km seismic discontinuity: Implications for mantle dynamics and differentiation. *Nature* 331: 131–136.

Ringwood AE (1994) Role of the transition zone and 660 km discontinuity in mantle dynamics. *Physics of Earth and Planetary Interiors* 86: 5–24.

Ross NL and Hazen RM (1990) High-pressure crystal chemistry of $MgSiO_3$ perovskite. *Physics and Chemistry of Minerals* 17: 228–237.

Ross NL, Shu JF, Hazen M, and Gasparik T (1990) High-pressure crystal chemistry of stishovite. *American Mineralogist* 75: 739–747.

Sanehira T, Irifune T, Shinmei T, Brunet F, Funakoshi K, and Nozawa A (2005) *In-situ* X-ray diffraction study of an aluminous phase in MORB under lower mantle conditions. *Physics and Chemistry of Minerals* 33: 28–34 (doi:10.1007/s00269-005-0043-0).

Santillán J and Williams Q (2004) A high pressure X-ray diffraction study of aragonite and the post-aragonite phase transition in $CaCO_3$. *American Mineralogist* 89: 1348–1352.

Sawamoto H (1987) Phase diagram of $MgSiO_3$ at pressures up to 24 GPa and temperatures up to 2200C: Phase stability and properties of tetragonal garnet. In: Manghnani MH and Syono Y (eds.) *High-Pressure Research in Mineral Physics*, pp. 209–219. Tokyo: Terrapub/AGU.

Saxena SK, Dubrovinsky LS, Lazor P, *et al.* (1996) Stability of perovskite ($MgSiO_3$) in the earth's mantle. *Science* 274: 1357–1359.

Sharp TG, El Goresy A, Wopenka B, and Chen M (1999) A post-stishovite SiO_2 polymorph in the meteorite Shergotty: Implications for impact events. *Science* 284: 1511–1513.

Shen G, Rivers ML, Wang Y, and Sutton R (2001) Laser heated diamond anvil cell system at the Advanced Photon Source for *in situ* X-ray measurements at high pressure and temperature. *Review of Scientific Instruments* 72: 1273–1282.

Sherman DM and Jansen H (1995) First-principles prediction of the high-pressure phase transition and electronic structure of FeO; implications for the chemistry of the lower mantle and core. *Geophysical Research Letters* 22: 1001–1004.

Shieh SR, Mao H-K, Hemley RJ, and Ming LC (1998) Decomposition of phase D in the lower mantle and the fate of dense hydrous silicates in subducting slab. *Earth and Planetary Science Letters* 159: 13–23.

Shieh SR, Duffy TS, and Li B (2002) Strength and elasticity of SiO_2 across the stishovite–$CaCl_2$-type structural phase boundary. *Physical Review Letters* 89: 255507.

Shieh SR, Duffy TS, and Shen G (2004) Elasticity and strength of calcium silicate perovskite at lower mantle pressures. *Physics of Earth and Planetary Interiors* 143-144: 93–105.

Shim S-H and Duffy TS (2000) Constraints on the *P–V–T* equation of state of $MgSiO_3$ perovskite. *American Mineralogist* 85: 354–363.

Shim S-H, Duffy TS, and Shen G (2000a) The stability and *P–V–T* equation of state of $CaSiO_3$ perovskite in the earth's lower mantle. *Journal of Geophysical Research* 105: 25955–25968.

Shim S-H, Duffy TS, and Shen G (2000b) The equation of state of $CaSiO_3$ perovskite to 108 GPa at 300 K. *Physics of Earth and Planetary Interiors* 120: 327–338.

Shim S-H, Duffy TS, and Shen G (2001a) The post-spinel transformation in Mg_2SiO_4 and its relation to the 660-km seismic discontinuity. *Nature* 411: 571–573.

Shim S-H, Duffy TS, and Shen G (2001b) Stability and structure of $MgSiO_3$ perovskite to 2300-kilometer depth in earth's mantle. *Science* 293: 2437–2440.

Shim S-H, Duffy TS, and Takemura K (2002a) Equation of state of gold and its application to the phase boundaries near 660 km depth in the Earth's mantle. *Earth and Planetary Science Letters* 203: 729–739.

Shim S-H, Jeanloz R, and Duffy TS (2002b) Tetragonal structure of $CaSiO_3$ perovskite above 20 GPa. *Geophysical Research Letters* 29: 2166.

Shim S-H, Duffy TS, Jeanloz R, and Shen G (2004) Stability and crystal structure of $MgSiO_3$ perovskite to the core–mantle boundary. *Geophysical Research Letters* 31: 10.1029/2004GL019639.

Shimomura O, Yamaoka S, Yagi T, *et al.* (1984) *Materials Research Society Symposium Proceedings, vol. 22: Multi-Anvil Type X-ray Apparatus for Synchrotron Radiation*, 17–20 pp. Amsterdam: Elsevier.

Shinmei T, Sanehira T, Yamazaki D, *et al.* (2005) High-temperature and high-pressure equation of state for the hexagonal phase in the system $NaAlSiO_4$–$MgAl_2O_4$. *Physics and Chemistry of Minerals* 32: 594–602 (doi:10.1007/s00269-005-0029-y).

Sidorin I, Gurnis M, and Helmberger DV (1999) Evidence for a ubiquitous seismic discontinuity at the base of the mantle. *Science* 286: 1326–1331.

Simmons NA and Gurrola H (2000) Seismic evidence for multiple discontinuities near the base of the transition zone. *Nature* 405: 559–562.

Sinmyo R, Hirose K, Hamane D, Seto Y, and Fujino K (2006) Partitioning of iron between perovskite/post-perovskite and magnesiowüstite in the Lower Mantle. *Eos Transactions of the American Geophysical Unioin* 87: Fall Meeting Supplement, Abstract MR11A-0105.

Sinogeikin SV and Bass JD (2000) Single-crystal elasticity of pyrope and MgO to 20 GPa by Brillouin scattering in the diamond cell. *Physics of Earth and Planetary Interiors* 120: 43–62.

Sinogeikin SV, Zhang J, and Bass JD (2004) Elasticity of single crystal and polycrystalline $MgSiO_3$ perovskite by Brillouin spectroscopy. *Geophysical Research Letters* 31: L06620 (doi:10.1029/2004GL019559).

Stacey FD and Isaak DG (2001) Compositional constraints on the equation of state and thermal properties of the lower mantle. *Geophysical Journal International* 146: 143–154.

Stackhouse S, Brodholt JP, Wookey J, Kendall J-M, and Price GD (2005a) The effect of temperature on the seismic anisotropy of the perovskite and post-perovskite polymorphs of $MgSiO_3$. *Earth and Planetary Science Letters* 230: 1–10.

Stackhouse S, Brodholt JP, and Price GD (2005b) High temperature elastic anisotropy of the perovskite and post-perovskite polymorphs of Al_2O_3. *Geophysical Research Letters* 32: L13305 (doi:10.1029/2005GL023163).

Stackhouse S, Brodholt JP, and Price GD (2006) Elastic anisotropy of $FeSiO_3$ end-members of the perovskite and post-perovskite phases. *Geophysical Research Letters* 33: L01304 (doi:10.1029/2005GL023887).

Stixrude L, Cohen RE, Yu R, and Krakauer H (1996) Prediction of phase transition in $CaSiO_3$ perovskite and implications for lower mantle structure. *American Mineralogist* 81: 1293–1296.

Sueda Y, Irifune T, Nishiyama N, *et al.* (2004) A new high-pressure form of $KAlSi_3O_8$ under lower mantle conditions. *Geophysical Research Letters* 31: L23612 (doi:10.1029/2004GL021156).

Sun S (1982) Chemical composition and the origin of the Earth's primitive mantle. *Geochimica et Cosmochimica Acta* 46: 179–192.

Suzuki A, Ohtani E, and Kamada T (2000) A new hydrous phase δ-AlOOH synthesized at 21 GPa and 1000°C. *Physics and Chemistry of Minerals* 27: 689–693.

Tackley PJ (2000) Mantle convection and plate tectonics: toward an integrated physical and chemical theory. *Science* 288: 2002–2007.

Tamai H and Yagi T (1989) High-pressure. and high-temperature phase relations in $CaSiO_3$ and $CaMgSi_20_6$ and elasticity. of perovskite-type $CaSiO_3$. *Physics of Earth and Planetary Interiors* 54: 370–377.

Tange Y (2006) The system MgO–FeO–SiO_2 up to 50 GPa and 2000°C: *An Application of Newly Developed Techniques Using Sintered Diamond Anvils in Kawai-Type High-Pressure Apparatus*, Doctoral Thesis, Tokyo Institute of Technology.

Tateno S, Hirose K, Sata N, and Ohishi Y (2005) Phase relations in $Mg_3Al_2Si_3O_{12}$ to 180 GPa: Effect of Al on post-perovskite phase transition. *Geophysical Research Letters* 32: L15306 (doi:10.1029/2005GL023309).

Taylor SR and McLennan SM (1985) *The Continental Crust: Its Composition and Evolution*, 312 pp. Oxford: Blackwell.

Thomson KT, Wentzcovitch RM, and Bukowinski M (1996) Polymorphs of Alumina predicted by first principles. *Science* 274: 1880–1882.

Tomioka N, Mori H, and Fujino K (2000) Shock-induced transition of $NaAlSi_3O_8$ feldspar into a hollandite structure in a L6 chondrite. *Geophysical Research Letters* 27: 3997–4000.

Trampert T, Deschamps F, Resovsky J, and Yuen D (2004) Probabilistic tomography maps chemical heterogeneities throughout the lower mantle. *Science* 306: 853–856.

Tsuchiya J, Tsuchiya T, and Tsuneyuki S (2002) First principles calculation of a high-pressure hydrous phase, δ-AlOOH. *Geophysical Research Letters* 29: 1909.

Tsuchiya J, Tsuchiya T, and Tsuneyuki S (2005a) First-principles study of hydrogen bond symmetrization of phase D under pressure. *American Mineralogist* 90: 44–49.

Tsuchiya J, Tsuchiya T, and Wentzcovitch RM (2005b) Vibrational and thermodynamic properties of $MgSiO_3$ post-perovskite. *Journal of Geophysical Research* 110: B02204 (doi:10.1029/2004JB003409).

Tsuchiya J, Tsuchiya T, and Wentzcovitch RM (2005c) Transition from the Rh_2O_3(II)-to-$CaIrO_3$ structure and the high-pressure–temperature phase diagram of alumina. *Physical Review B* 72: 020103(R) (doi:10.1103/PhysRevB.72.020103).

Tsuchiya T and Kawamura K (2001) Systematics of elasticity: *Ab initio* study in B1-type alkaline earth oxides. *Journal of Chemical Physics* 114: 10086–10093.

Tsuchiya T (2003) First-principles prediction of the *P–V–T* equation of state of gold and the 660-km discontinuity in Earth's mantle. *Journal of Geophysical Research* 108: 2462 (doi:10.1029/2003JB002446).

Tsuchiya T, Tsuchiya J, Umemoto K, and Wentzcovitch RM (2004a) Phase transition in $MgSiO_3$ perovskite in the Earth's lower mantle. *Earth and Planetary Science Letters* 224: 241–248.

Tsuchiya T, Tsuchiya J, Umemoto K, and Wentzcovitch RM (2004b) Elasticity of post-perovskite $MgSiO_3$. *Geophysical Research Letters* 31: L14603 (doi:10.1029/2004GL020278).

Tsuchiya T, Caracas R, and Tsuchiya J (2004c) First principles determination of the phase boundaries of high-pressure polymorphs of silica. *Geophysical Research Letters* 31: L11610 (doi:10.1029/2004GL019649).

Tsuchiya T and Tsuchiya J (2006) Effect of impurity on the elasticity of perovskite and postperovskite: Velocity contrast across the postperovskite transition in (Mg,Fe,Al) $(Si,Al)O_3$.

Geophysical Research Letters 33: L12S04 (doi:10.1029/2006GL025706).

Tsuchiya T, Wentzcovitch RM, and de Gironcoli S (2006) Spin transition in magnesiowüstite in Earth's lower mantle. *Physical Review Letters* 96: 198501.

Tutti F, Dubrovinsky LS, and Saxena SK (2000) High pressure phase transformation of jadeite and stability of $NaAlSiO_4$ with calcium-ferrite type structure in the lower mantle conditions. *Geophysical Research Letters* 27: 2025–2028.

Tutti F, Dubrovinsky LS, Saxena SK, and Carlson S (2001) Stability of $KAlSi_3O_8$ hollandite-type structure in the Earth's lower mantle conditions. *Geophysical Research Letters* 28: 2735–2738.

Umemoto K, Wentzcovitch RM, and Allen PB (2006) Dissociation of $MgSiO_3$ in the cores of gas giants and terrestrial exoplanets. *Science* 311: 983–986.

van der Hilst R, Widiyantoro S, and Engdahl E (1997) Evidence for deep mantle circulation from global tomography. *Nature* 386: 578–584.

Vinnik L, Kato M, and Kawakatsu H (2001) Search for seismic discontinuities in the lower mantle. *Geophysical Journal International* 147: 41–56.

Wang W and Takahashi E (1999) Subsolidus and melting experiments of a K-rich basaltic composition to 27 GPa: Implication for the behavior of potassium in the mantle. *American Mineralogist* 84: 357–361.

Wang Y, Weidner DJ, and Guyot F (1996) Thermal equation of state of $CaSiO_3$ perovskite. *Journal of Geophysical Research* 101: 661–672.

Wang Y, Uchida T, Von Dreele R, *et al.* (2004) A new technique for angle-dispersive powder diffraction using an energy-dispersive setup and synchrotron radiation. *Journal of Applied Crystallography* 37: 947–956.

Weidner DJ and Wang Y (2000) Phase transformations: implications for mantle structure. In: Karato S, Forte AM, Liebermann RC, Masters G, and Stixrude L (eds.) *Geophysical Monograph*, vol. 117, pp. 215–235. Washington, DC: American Geophysical Union.

Wentzcovitch RM, Ross NL, and Price GD (1995) *Ab initio* study of $MgSiO_3$ and $CaSiO_3$ perovskites at lower-mantle pressures. *Physics of Earth and Planetary Interiors* 90: 101–112.

Wentzcovitch RM, Stixrude L, Karki BB, and Kiefer B (2004) Akimotoite to perovskite phase transition in $MgSiO_3$. *Geophysical Research Letters* 31: L10611 (doi:10.1029/2004GL019704).

Wentzcovitch RM, Tsuchiya T, and Tsuchiya J (2006) $MgSiO_3$ postperovskite at D″ conditions. *Proceedings of the National Academy of Sciences USA* 103: 543–546.

Williams Q (1998) The temperature contrast across D″. In: Gurnis M, Wysession ME, Knittle E, and Buffett BA (eds.) *The Core-Mantle Boundary Region, pp.73–81*. Washington, DC: AGU.

Wood BJ and Rubie DC (1996) The effect of alumina on phase transformations at the 660-kilometer discontinuity from Fe-Mg partitioning experiments. *Science* 273: 1522–1524.

Wood BJ (2000) Phase transformations and partitioning relations in peridotite under lower mantle conditions. *Earth and Planetary Science Letters* 174: 341–354.

Wookey J, Stackhouse S, Kendall J-M, Brodholt JP, and Price GD (2005) Efficacy of the post-perovskite phase as an explanation of lowermost mantle seismic properties. *Nature* 438: 1004–1008.

Wysession ME, Lay T, Revenaugh J, *et al.* (1998) The D″ discontinuity and its implications. In: Gurnis M, Wysession ME, Knittle E, and Buffett BA (eds.) *The Core–Mantle Boundary Region*, pp. 273–298. Washington: DC AGU.

Yagi T, Mao HK, and Bell PM (1982) Hydrostatic compression of perovskite-type $MgSiO_3$. In: Saxena K (ed.) *Advances on Physical Geochemistry*, vol.2, pp. 317–325. New York: Springer-Verlag.

Yagi T, Suzuki T, and Akaogi M (1994) High pressure transitions in the system $KAlSi_3O_8$-$NaAlSi_3O_8$. *Physics and Chemistry of Minerals* 21: 387–391.

Yang H, Prewitt CT, and Frost DJ (1997) Crystal structure of the dense hydrous magnesium silicate, phase D. *American Mineralogist* 82: 651–654.

Yamazaki D and Karato S (2002) Fabric development in (Mg,Fe)O during large strain, shear deformation: Implications for seismic anisotropy in Earth's lower mantle. *Physics of Earth and Planetary Interiors* 131: 251–267.

Yeganeh-Haeri A, Weidner DJ, and Ito E (1989) Elasticity of $MgSiO_3$ in the perovskite structure. *Science* 248: 787–789.

Yu YG, Wentzcovitch RM, Tsuchiya T, Umemoto K, and Tsuchiya J (2006) First Principles Investigation of Ringwoodite's Dissociation. *Geophysical Research Letters* (submitted).

Zhao D (2004) Global tomographic images of mantle plumes and subducting slabs: insight into deep Earth dynamics. *Physics of Earth and Planetary Interiors* 146: 3–34.